Title

Oxidized phospholipids are proinflammatory and proatherogenic in hypercholesterolaemic mice.

Journal

Nature, 558(7709)

ISSN

0028-0836

Authors

Que, Xuchu
Hung, Ming-Yow
Yeang, Calvin
et al.

Publication Date

2018-06-06

DOI

10.1038/s41586-018-0198-8

Peer reviewed

HHS Public Access

Author manuscript

Nature. Author manuscript; available in PMC 2018 December 06.

Published in final edited form as:

Nature. 2018 June ; 558(7709): 301–306. doi:10.1038/s41586-018-0198-8.

Oxidized Phospholipids are Proinflammatory and Proatherogenic in Hypercholesterolemic Mice

Xuchu Que[1], **Ming-Yow Hung**[1,*], **Calvin Yeang**[1], **Ayelet Gonen**[1], **Thomas A. Prohaska**[1], **Xiaoli Sun**[1], **Cody Diehl**[1,**], **Antti Määttä**[2], **Dalia E. Gaddis**[3], **Karen Bowden**[1], **Jennifer Pattison**[1], **Jeffrey G. MacDonald**[4], **Seppo Ylä-Herttuala**[2], **Pamela L. Mellon**[5], **Catherine C. Hedrick**[3], **Klaus Ley**[3], **Yury I Miller**[1], **Christopher K Glass**[1,6], **Kirk L. Peterson**[1], **Christoph J. Binder**[7,8], **Sotirios Tsimikas**[1], and **Joseph L. Witztum**[1]

[1]Dept. of Medicine, University of California, San Diego, La Jolla, CA, USA [2]A.I. Virtanen Institute, University of Eastern Finland, Finland [3]La Jolla Institute for Allergy and Immunology, La Jolla, CA, USA [4]Center for Human Nutrition, UT Southwestern Medical Center, Dallas, TX USA [5]Dept of Reproductive Medicine, University of California, San Diego, La Jolla, CA, USA [6]Dept of Cellular and Molecular Medicine, University of California, San Diego, La Jolla, CA, USA [7]Dept. of Laboratory Medicine, Medical University of Vienna, Vienna, Austria [8]Center for Molecular Medicine of the Austrian Academy of Sciences, Vienna, Austria

Keywords

Oxidized phospholipids; Natural antibodies; Atherosclerosis; Inflammation; Hepatosteatosis

INTRODUCTION

Oxidized phospholipids (OxPL) are ubiquitous, formed in many inflammatory tissues, including atherosclerotic lesions, and frequently mediate proinflammatory changes[1]. Because OxPL are mostly products of non-enzymatic lipid peroxidation, mechanisms to specifically neutralize them are unavailable and their roles *in vivo* are largely unknown. We previously cloned the IgM natural antibody E06, which binds the phosphocholine (PC) headgroup of OxPL and blocks the uptake of OxLDL by macrophages and inhibits proinflammatory properties of OxPL[2-4]. To determine the role of OxPL *in vivo* in the context of atherogenesis, we generated transgenic mice in the *Ldlr*$^{-/-}$ background that

Correspondence: Joseph L Witztum, MD Department of Medicine, University California San Diego, Biomedical Science Building-Room 1080, 9500 Gilman Drive La Jolla, CA 92093-0682. jwitztum@ucsd.edu.

*Current address: Division of Cardiology, Dept. of Internal Medicine, Shuang Ho Hospital, Taipei Medical University, New Taipei City, Taiwan; Dept. of Internal Medicine, School of Medicine, College of Medicine, Taipei Medical University, Taipei City, Taiwan

**Current address: Brigham Young University Idaho, Rexburg, ID, USA

Author Contributions X.Q.,S.T., J.L.W. designed the project, X.Q., A.G., T.A.P., X.S., C.D., A.M., D.E.G., K.B., J.P. and J.G.M. conducted key experiments; P.L.M., C.C.H., K.L.P. and C.K.G. provided vital technical expertise and advice; M-Y.H., C.Y., K.L.P., and S.T. conducted aortic valve studies; and X.Q. and J.L.W. wrote the manuscript with expert input from C.K.G., Y.I.M., S.Y-H., C.J.B., S.T. and all coauthors.

expressed a single-chain variable fragment of E06 (E06-scFv) using the *apo*E promoter. The E06-scFv was secreted into plasma from liver and macrophages, and achieved sufficient plasma levels to inhibit *in vivo* macrophage uptake of OxLDL and OxPL-induced inflammatory signaling. Compared to *Ldlr*$^{-/-}$, *Ldlr*$^{-/-}$/E06-scFv mice had less atherosclerosis by 57-28% after 4, 7, and even 12 months respectively of 1% high-cholesterol diet (HCD). Echocardiographic and histologic evaluation of aortic valves (AV) demonstrated that E06-scFv ameliorated the development of AV gradients and decreased AV calcification. Both cholesterol accumulation and *in vivo* uptake of OxLDL were decreased in peritoneal macrophages, and both peritoneal and aortic macrophages had a decreased inflammatory phenotype. Serum amyloid A was decreased 32% indicating decreased systemic inflammation, and hepatic steatosis and inflammation were also decreased. Finally, the E06-scFv prolonged life as measured over 15 months. Because the E06-scFv lacks functional effects of an intact antibody other than the ability to bind OxPL and inhibit OxLDL uptake in macrophages, these data support a major proatherogenic role of OxLDL and demonstrate that OxPL are proinflammatory and proatherogenic, which E06 counteracts *in vivo*. These studies suggest that therapies inactivating OxPL may be beneficial in reducing generalized inflammation, including the progression of atherosclerosis, aortic stenosis and hepatic steatosis.

Oxidation of LDL (OxLDL), a central event in atherogenesis, results in formation of neo-epitopes from lipid peroxidation, termed “oxidation-specific-epitopes” (OSE), which are endogenous “danger-associated molecular patterns” recognized by multiple innate pattern recognition receptors[1,5]. Phosphocholine (PC) containing oxidized phospholipids (OxPL) are a prominent example, and the PC headgroup of OxPL in OxLDL (as a lipid or OxPL-protein adduct) is recognized by macrophage scavenger receptors and TLRs, by innate protein CRP and by the IgM natural antibody (NAb) E06[1]. OxPLs accumulate in OxLDL, apoptotic cells and microparticles released by activated and dying cells[4,6] and are ubiquitous in a wide variety of inflammatory settings, including atherosclerosis[7], pulmonary[8,9] and neurological diseases[10-12] and NASH[13] among others[1]. In addition, OxPL present on Lp(a) are thought to mediate, in part, the ability of Lp(a) to promote atherogenesis and calcific aortic valve disease (CAVD)[14]. However, the pathophysiological effects of endogenously generated OxPL *in vivo* are unknown and it is unlikely that they could be specifically neutralized *in vivo* by small molecules or enzyme inhibitors.

The NAb E06 recognizes the hydrophilic PC headgroup of OxPLs present in OxLDL and apoptotic cells but does not recognize unoxidized PL in LDL or viable cells. Furthermore, E06 blocks uptake of OxLDL by macrophages *in vitro* and can inhibit many proinflammatory properties of OxPL (A detailed characterization of E06 can be found in Supplementary Information). To determine the role of OxPL *in vivo* in atherogenesis, we generated transgenic mice expressing a single chain variable fragment of E06 (E06-scFv) as described in Methods (Extended Data Fig. 1a-c). The E06-scFv cDNA was inserted into a liver-specific expression vector, pLiv7, under the *apo*E promoter and a hepatic control element enhancer (LE6) (Fig. 1a) and used to generate E06-scFv transgenic mice in the C57BL/6 background. These were crossbred to generate “homozygous” mice, which were bred into *Ldlr*$^{-/-}$ and *Rag1*$^{-/-}$/*Ldlr*$^{-/-}$ mice on the C57BL/6 background. The *E06-scFv* mRNA exhibited highest expression in liver, macrophages and spleen, and low-level

expression in heart, lung, kidney, and brain. (Extended Data: Fig. 1d). The plasma E06-scFv levels in the various transgenic models studied were ~20-30 μg/mL. Plasma titers of the endogenous IgM E06 were not affected by the E06-scFv transgene in the various studies described (Extended Data: Fig. 2). Binding and competition studies validated that plasma E06-scFv fully replicated the binding properties of the parent E06 IgM, specifically binding to various PC epitopes as well as OxLDL and a POVPC-peptide, (a synthetic OxPL-peptide analogue[15]) and to AB1-2, a highly specific T15/E06 anti-idiotypic Ab (Fig. 1b and Extended Data: 1e). Even at high dilutions (1:100), plasma from *Ldlr*$^{-/-}$/E06-scFv mice inhibited binding of biotinylated OxLDL to J774 macrophages in culture by > 75% (Fig. 1c). E06-scFv also inhibited the proinflammatory activation of thioglycollate elicited macrophages (TGEM) when oxidized PAPC (OxPAPC) was injected *in vivo*. Expression of both TNFα and IL-1β was markedly attenuated in TGEM from the *Ldlr*$^{-/-}$/E06-scFv mice (Fig. 1d). E06-scFv enriched plasma bound to rabbit atherosclerotic tissue (Extended Data: Fig. 3a), and also prominently stained late stage apoptotic cells but not viable cells (Extended Data: Fig. 3b and c). PC-KLH effectively abolished E06-scFv binding in both cases (data not shown). We also demonstrated the presence of E06-scFv antibody in aortic roots of *Ldlr*$^{-/-}$/E06-scFv mice, consistent with either plasma origin or local macrophage secretion (Extended Data: Fig. 3d).

To determine the impact of OxPL on atherosclerosis, *Ldlr*$^{-/-}$ and *Ldlr*$^{-/-}$/E06-scFv mice were fed a HCD for 4, 7 or 12 months. Weight gain, plasma cholesterol, triglycerides and lipoprotein profiles were similar (Extended Data: Table 1 and Fig. 4). Compared to *Ldlr*$^{-/-}$ mice, atherosclerosis was significantly reduced in *Ldlr*$^{-/-}$/E06-scFv mice at each time point (*en face* by 57%, 34% and 28%, and aortic root by 55%, 41% and 27% respectively) (Fig. 2c and d). OxPL promote apoptosis and necrosis[1,16] In lesion size-matched cross sections, necrotic core areas were 44% smaller (p=0.015) and had visibly more collagen in *Ldlr*$^{-/-}$/E06-scFv mice, suggesting improved plaque stability (Extended Data: Fig. 5a).

The *apoE* promoter is known to be active in macrophages and to respond to cholesterol and LXR agonists[17]. Peritoneal macrophages from *Ldlr*$^{-/-}$/E06-scFv mice expressed E06-scFv mRNA, and ELISA analysis of culture supernatants demonstrated the binding of secreted E06-scFv to PC-BSA (Extended Data: Fig. 5b). The LXR agonist T0901317 enhanced synthesis and secretion of bioactive E06-scFv into the culture media (Extended Data: 5b), demonstrating a functional *apo*E promoter regulating expression of the E06-scFv in macrophages. To determine the contribution of macrophage E06-scFv to atherogenic protection, we performed a bone marrow transplantation (BMT) from C57BL/6 wildtype or from E06-scFv mice (not on *Ldlr*$^{-/-}$ background) into irradiated male *Ldlr*$^{-/-}$ recipients and fed the mice with a western diet (WD). Plasma E06-scFv titers were detectable in recipient *Ldlr*$^{-/-}$ mice 2 weeks after BMT and rose in response to cholesterol feeding (Extended Data: Fig. 5c), but even at 16 weeks were only ~10% of those observed in the *Ldlr*$^{-/-}$/E06-scFv mice. Nevertheless, aortic root lesions were reduced by 37% in mice receiving BM from E06-scFv donors, compared to wildtype donors (Extended Data: 5d). Plasma lipids were not different (Extended Data: Table 1). These data suggest an important role for local arterial macrophage secretion of E06-scFv in providing atheroprotection, though conceivably some of the E06-scFv's benefit could derive from macrophages engrafted in other tissues.

To provide insight into atheroprotective mechanisms, we demonstrated decreased *in vivo* macrophage uptake of fluorescently-labeled OxLDL in *Ldlr*$^{-/-}$Æ06-scFv mice. We used *Rag1*$^{-/-}$/*Ldlr*$^{-/-}$ mice to exclude effects of other antibodies and allow an examination of the protective effect of the E06-scFv alone. Uptake of OxLDL was significantly reduced in macrophages of *Rag1*$^{-/-}$/*Ldlr*$^{-/-}$Æ06-scFv compared to *Rag1*$^{-/-}$/*Ldlr*$^{-/-}$ mice (Fig. 3a). To assess the full potential of E06-scFv to bind to OxLDL, we pre-incubated plasma from *Ldlr*$^{-/-}$ or *Rag1*$^{-/-}$/*Ldlr*$^{-/-}$ or *Rag1*$^{-/-}$/*Ldlr*$^{-/-}$Æ06-scFv mice with the OxLDL before injection. Whereas uptake of OxLDL was ~ 100% and ~70% for the OxLDL incubated with *Rag1*$^{-/-}$ or *Rag1*$^{-/-}$/*Ldlr*$^{-/-}$ plasma respectively, it was reduced to ~ 26% when premixed with *Rag1*$^{-/-}$/*Ldlr*$^{-/-}$Æ06-scFv plasma (Fig. 3b). Consistent with the decreased *in vivo* uptake of OxLDL, macrophage cholesterol content of *Ldlr*$^{-/-}$Æ06-scFv mice was reduced 48% compared to *Ldlr*$^{-/-}$ mice. (p=0.02) (Fig. 3c). Desmosterol was reported to be increased in macrophages from WD fed *Ldlr*$^{-/-}$ mice, leading to decreased inflammatory gene expression[18]. However, neither desmosterol nor other oxysterol concentrations were different between macrophages of *Ldlr*$^{-/-}$ and *Ldlr*$^{-/-}$Æ06-scFv mice (Extended Data: Fig. 1f).

RNAseq analysis of TGEM (Fig. 3d and e) suggested a shift from a more inflammatory "M1-like" phenotype in the *Ldlr*$^{-/-}$ mice to a more attenuated "M2-like" repair phenotype in the *Ldlr*$^{-/-}$Æ06-scFv mice. Gene Ontology (GO) analyses indicated that nearly all the genes expressed >1.5-fold higher in the *Ldlr*$^{-/-}$Æ06-scFv macrophages relate to immune regulation and defense, both innate and adaptive (Extended Data: Table 2). We also utilized flow cytometry to profile arterial wall cells (Fig. 3f). Compared to macrophages isolated from aortas of chow-fed *Ldlr*$^{-/-}$ mice, macrophages from HCD *Ldlr*$^{-/-}$ mice were shifted to a predominant "M1-like" phenotype ($CD45^+CD11b^+CD11c^+$ $Arg1^-$), whereas despite the same cholesterol levels, macrophages from the HCD *Ldlr*$^{-/-}$Æ06-scFv mice showed an M2-like phenotype ($CD45^+CD11b^+CD11c^-Arg1^+$), more comparable to that seen in the chow-fed *Ldlr*$^{-/-}$ mice.

Aortas from HCD fed *Ldlr*$^{-/-}$ mice had greater total monocyte/lymphocyte accumulation than did chow-fed *Ldlr*$^{-/-}$ or HCD *Ldlr*$^{-/-}$Æ06-scFv mice, and in particular, a greater enrichment of lymphocytes, especially T but also B cells (Extended Data: Table 3). The proportions of CD4+ and CD8+ T cells in blood, peri-aortic lymph nodes and spleens of *Ldlr*$^{-/-}$ and *Ldlr*$^{-/-}$Æ06-scFv mice were not different (data not shown). There were no differences between the two groups in blood RBC or WBC counts, nor in blood coagulation markers including PT and aPTT, fibrinogen, and plasminogen (data not shown).

Recent genetic data demonstrate a strong causal role for Lp(a) and its associated OxPL in the etiology of CAVD in humans[14,19]. We therefore prospectively used 2D and Doppler ultrasound, to measure gradients at the AV in HCD *Ldlr*$^{-/-}$ and *Ldlr*$^{-/-}$Æ06-scFv mice at 6, 9 and 12 months, and at 15 months, the AV calcium content was evaluated histologically. There was a progressive increase over time in mean AV pressure gradients in *Ldlr*$^{-/-}$ mice, which was significantly attenuated in the *Ldlr*$^{-/-}$Æ06-scFv mice and was 49% lower at 12-months (Fig. 4a, and Extended Data: Fig. 6a and Table 4). Total AV calcium content was also significantly reduced by 41.5% (Fig. 4b and c). Consistent with the more extensive pathology noted in the AV leaflets in the *Ldlr*$^{-/-}$ mice (Fig. 4b and Extended Data: Fig 5a)

representative M-mode echocardiography demonstrated thicker AV valves in the *Ldlr*$^{-/-}$ mice (Extended Data: Fig. 6b). Over 15 months of prospective observation, it was notable that 6 of 13 *Ldlr*$^{-/-}$ mice died, whereas 0 of 10 *Ldlr*$^{-/-}$Æ06-scFv mice died (p = 0.016 via Kaplan-Meier survival analysis) (Fig. 4d).

Livers of mice on a HCD diet are known to develop steatosis and accumulate enhanced levels of OSE, including OxPL[20]. Livers from *Ldlr*$^{-/-}$ mice stained prominently with E06 IgM compared to *Ldlr*$^{-/-}$Æ06-scFv livers (Fig. 4f), though hepatocyte derived E06-scFv may partially mask OxPL epitopes in the *Ldlr*$^{-/-}$Æ06-scFv mice. The histological appearance of steatosis in the *Ldlr*$^{-/-}$Æ06-scFv livers was decreased, which was confirmed by significant decreases in hepatic triglyceride and cholesterol content (Fig. 4e), and there was decreased inflammatory gene expression in whole liver extracts (Extended Data: Fig. 6c).

Serum Amyloid A (SAA) is known to be raised by cholesterol feeding and reflects systemic inflammatory status in mice[21]. Remarkably, despite plasma cholesterol values >800 mg/dL, plasma SAA levels were reduced 32% in *Ldlr*$^{-/-}$Æ06-scFv mice (p=0.016) supporting a generalized decrease in systemic inflammation (Fig. 4g).

The detailed cellular and molecular mechanisms by which OxPL mediate these proatherogenic and proinflammatory effects are likely to be complex, dependent on the diverse OxPLs and different cellular targets involved. For example, OxPLs can activate cells by a variety of receptors, including CD36, TLR2/1 and 6, TLR4, CD14 and combinations of these receptors, and in turn, generate a wide variety of responses[1,5,7,8,16,22-25]. In addition, the PC on OxLDL mediates macrophage uptake by CD36 and SR-B1[5]. Presumably, extracellular E06-scFv binds to many of the extracellular OxPL moieties formed and by blocking uptake of OxLDL and inhibiting inflammatory signaling, contributes to reduced atherogenesis, though we cannot exclude the possibility that the E06-scFv in the intracellular signaling pathway of macrophages or hepatocytes may also contribute in some manner.

In summary, we present a unique murine model that demonstrates that in the context of hypercholesterolemia, OxPL are involved in the pathogenesis of inflammation in general, and atherosclerosis, CAVD and hepatic steatosis specifically. CAVD is a growing problem in our aging population and leads to symptomatic aortic stenosis requiring AV replacement by surgical or trans-catheter approaches in > 2% of those over age 65[26]. Similarly, OxPL may be involved in the pathogenesis of NASH, which currently afflicts a high percentage of the population and increases the risk for cirrhosis and cardiovascular disease. The E06 transgenic mice can be used to study the mechanisms by which OxPL contributes to these disease processes *in vivo*, as well as other disease states in which OxPL may play a role. For example, we recently demonstrated with these mice that OxPL restrains bone formation in mice fed either a WD or chow diet[27].

This unique sensitivity of E06 to molecules with abnormally presented PC may allow specific therapeutic targeting of diseased tissues but not normal tissues in a variety of inflammatory states. As shown here as proof-of-principle, diseases of systemic inflammation that generate OxPL may be targets of OxPL-directed therapies. Furthermore, OxPL in

various tissues can be imaged with OxPL specific antibodies, such as in atherosclerotic aortas using MRI-based nanoparticles[28], which could aid in the appropriate selection of high-risk patients. The E06-scFv expressed in these mice lacks Fc effector functions of antibodies, and therefore, its impact was caused solely by blocking biological effects of OxPL. Translational applications of E06 or similar anti-OxPL antibodies to humans, as well as antibodies to other OSE[29,30], in which more traditional IgG isotypes are more likely to be used, will need to decipher any potential additional roles of various Fc effector functions.

MATERIALS AND METHODS

Antigen preparation and modifications

Plasma was obtained from healthy donors after an overnight fast following consent under a protocol approved by the UCSD Human Research Protections Program. LDL was isolated by sequential ultracentrifugation, and modified with malondialdehyde (MDA), malondialdehyde-acetaldehyde-adducts (MAA) or CuSO4 to generate MDA-LDL, MAA-LDL or copper-oxidized LDL (Cu-OxLDL) respectively, as previously described[31]. Phosphocholine-BSA (PC-BSA) was from Biosearch Technologies and POVPC-BSA was prepared as described[32]. Monoclonal anti-Myc and anti-His alkaline phosphatase (AP) conjugated antibodies were from Sigma.

E06-scFv construction and optimized expression

In the Supplementary Information, we describe in detail the history of the discovery of the IgM natural antibody E06/T15 and its binding specificity and biological properties. The cDNAs encoding the E06 variable heavy (V_H) and Light (L_H) regions were connected with an oligo linker of 15-amino acid peptide (Gly4Ser)3 that were assembled by overlapping PCR and cloned into an expression vector pSecTag2A (Invitrogen), which contains a murine Ig kappa-chain leader sequence for secretion and Myc and polyHis tags that facilitates purification and detection. HEK293 cells were transfected with pSecTag2A-E06-scFv plasmid using the lipofectamine plus reagent (Invitrogen). Stable transfectants were selected with Zeocin, and the E06-scFv antibody in the culture supernatant was identified using an ELISA plate pre-coated with Cu-OxLDL or PC-BSA and detection by anti-myc or anti-His tag antibody conjugate using chemiluminescent assay techniques described previously[29]. During development, multiple linkers were tried and in addition, site-directed mutagenesis in framework region 1 was performed at 7 sites in an iterative fashion using QuickChange Multi Site-Directed Mutagenesis Kit (Stratagene) to create point mutations to improve the folding, stability, yield and reduce the aggregation of recombinant scFv. His6-tagged E06-scFv was purified on Ni-NTA agarose beads (Qiagen) according to the manufacture's protocols. Briefly, cell lysates were clarified by centrifugation (20,000 × g, 30 min, 4°C), and the supernatant applied to Ni^{2+}-NTA agarose column, from which His6-tagged E06-scFv was eluted with 250 mM imidazole. Fractions containing E06-scFv were pooled and extensively dialyzed against PBS before use. The purity and integrity were assessed by SDS-PAGE and Western blot with anti-His Tag Ab-HRP conjugate, and an ECL detection system (Amersham).

Generation of E06-scFv transgenic mice

The liver-specific expression vector pLiv7 was used to generate transgenic mice expressing the E06-scFv transgene driven by the *apo*E promoter, as previously reported[33]. The *Mfe*I-*Mlu*I fragment from the pSecTag2A-E06-scFv plasmid including murine Ig kappa leader sequence and Myc/His tags was released by *Mfe*I/*Mlu*I digestion, and inserted into the polylinker region of pLiv7 to generate a transgenic vector pLiv7-E06-scFv. The apoE-E06-scFv transgene consists of 3.0 kb *ApoE* promoter, and 5′, 3′-UTR of *apo*E flanked E06-scFv gene and a 0.77 kb hepatic control element (LE6) placed downstream of poly(A) signal (Fig 1). To create transgenic mice, a 6.8 kb apoE-E06-scFv transgene cassette was separated from the vector by digestion with *sac*II and *spe*I, purified, and injected into the pronuclei of fertilized mouse eggs obtained from superovulated female mice (C57BL/6). The injected eggs were surgically transferred to oviducts of surrogate C57BL/6 females in the UCSD Transgenic and Knockout Mouse Core.

Production and screening of transgenic mice

Offspring were screened both for plasma E06-scFv titer and integration of the transgene by PCR amplification of the tail DNA with the upstream primer sequence MfeFw 5′-TAC AAT TGA GCT GGC TAG CCA CCA TGG AG-3′ and the downstream E06rev3 primer sequence 5′-GCT GTA CCA AGC CTC CTC CAG ACT CCA CCA G-3′ to yield a 540-bp product corresponding to the nucleotide sequence between −15 and 525 of E06-scFv cDNA. Mice from the highest expressing transgenic E06-scFv founder lines were bred with each other to generate "homozygous" transgenic mice, and in turn, these were crossed into *Ldlr*$^{-/-}$ and *Ldlr*$^{-/-}$ *Rag1*$^{-/-}$ mice, all on the C57BL/6 background. All animals were genotyped for E06-scFv and *Ldlr*$^{-/-}$, respectively and plasma assayed to confirm expression of the E06-scFv by immunoassay.

Binding profile of plasma E06-scFv quantified by chemiluminescent ELISA

E06-scFv plasma titers were determined by chemiluminescent ELISA assays for binding to PC epitopes as expressed on Cu-OxLDL, PC-KLH, PC-BSA,POVPC-BSA, and capsular polysaccharide (C-PS) of *S. pneumonia*, as well as to the anti-T15 idiotype antibody AB1-2[2]. Competition immunoassays were performed to demonstrate specificity[31,32] In brief, 96-well round-bottomed MicroFluor plates (DYNEX Technologies, Chantilly, VA) were coated with various antigens at 5 μg/mL (50 μL per well) in PBS overnight at 4°C. After the plates were washed and blocked with 1% BSA-TBS for 30 min, 25 μL of primary Abs diluted with 1% BSA-PBS were added to the wells, in the absence or presence of competitors and incubated for 90 min at room temperature. Bound Abs were detected with anti-Hisx6 tag antibody conjugated with alkaline phosphatase (SIGMA), in Tris buffered saline (TBS) buffer containing 1% BSA, followed by a rinse with water and the addition of 25 μL of 50% LumiPhos 530 (Lumigen, Southfield, MI) as luminescent substrate. The light emissions were measured, and counts expressed as relative light units (RLU) over 100 ms using a Dynex Luminometer (DYNEX Technologies). For competition immunoassays, data are expressed as B/B_0, were B represents binding in presence and B_0 in absence of competitors. In separate experiments, the absolute plasma E06-scFv levels in transgenic

mice were determined using a standard curve generated with purified His6-tagged E06-scFv isolated as described above. All determinations were done in triplicate.

Flow cytometry and deconvolution microscopy of E06-scFv-Tg plasma binding to apoptotic cells

Plasma of *Ldlr*$^{-/-}$/E06-scFv-Tg and *Ldlr*$^{-/-}$ control mice were analyzed for binding to apoptotic cells by flow cytometry (FACS) analysis as described[4]. Thymocytes harvested from C57BL/6 mice were cultured in cell culture medium and induced to undergo apoptosis by 10 ng/ml PMA (Sigma-Aldrich) for 16 hours. Plasmas diluted in 1% BSA-PBS were incubated with apoptotic thymocytes for 1hr at 4°C, followed by incubation with FITC-labeled anti-His6 mAb in 1% BSA-PBS for 30 minutes at 4°C. Apoptotic cells were double-stained with Annexin V - Phycoerythrin (Annexin V - PE) and 7-amino-actinomycin (7-AAD) (BD Biosciences) for 15 min and immediately analyzed by FACS using a FACSCanto (BD Biosciences). For immunofluorescence microscopy studies, apoptotic Jurkat cells were prepared by exposure to UV irradiation at 20 mJ/cm2, and further cultured for 16 hours before use. Apoptotic Jurkat cells were incubated with 100 μL of plasma (1:20) in 1% BSA-PBS at 4°C for 1hr, washed and labeled with FITC-conjugated anti-His-tag mAb (1:1000) and 1 μg/mL of Hoechst dye (Sigma-Aldrich) for 45 min at 4°C. The cells were fixed with 3.7% paraformaldehyde for 20 min, washed, and resuspended in 1% BSA-PBS. The cells were spun down on glass slides using cytospin (Thermo Shandon). Images were captured using a DeltaVision deconvolution microscopic system operated by SoftWorx software (Applied Precision) as described previously.

Demonstration of specificity of E06-scFv binding to OxPL and ability to inhibit OxLDL binding to macrophages

Binding of biotinylated OxLDL to J774 macrophages plated in microtiter wells was assessed by a chemiluminescent binding assay as described recently[34]. In brief: biotinylated Cu-OxLDL (5 μg/ml) was incubated in the absence or presence of E06-scFv-Tg plasma or control at various dilutions overnight at 4°C. The supernatants were then added to macrophages plated in 96-well microtiter plates and the binding of biotinylated OxLDL detected by AP-labeled NeutrAvidin and chemiluminescent ELISA.

Impact of E06-scFv on atherosclerosis in *Ldlr*$^{-/-}$ mice

Animal protocols were approved by the Institutional Animal Care and Use Committee (IACUC) at University of California San Diego. At 8 weeks of age, 18-20g male *Ldlr*$^{-/-}$ or *Ldlr*$^{-/-}$/E06-scFv-Tg mice were matched for age, body weight, and total cholesterol and placed on a 1% cholesterol diet (HCD) (TD97131, Harlan Teklad) to determine the impact of the E06-scFv on progression of atherosclerosis. For each study, we sought to have 8-10 mice per group, which based on experience would be sufficient to detect differences in atherosclerosis. Blood samples were collected from submandibular bleeding at 0, and various time points on diet. Mice were weighed monthly, and total cholesterol and triglycerides levels were determined using automated enzymatic assays (Roche Diagnostics, Indianapolis). Lipoprotein profiling was performed on terminal blood samples using fast performance liquid chromatography (FPLC) equipped with a Superose 6 column, and total cholesterol and triglycerides levels in each fraction were determined as described[29].

Bone marrow transplantation (BMT) study

BMT was performed as previously described[35]. In brief, bone marrow (BM) was harvested from cleaned femurs and tibias of male E06-scFv mice (not on *Ldlr*$^{-/-}$ background) and wildtype C57BL/6 mice and re-suspended in RPMI 1640 medium for injection. *Ldlr*$^{-/-}$ male recipient mice were fasted overnight and received a lethal dose of radiation (9 Gy) 4 h before BM injection. Mice (n = 12 per group) were anesthetized with isoflurane, and 5×10^6 BM cells either from E06-scFv mice or from C57BL/6 wildtype mice were injected into the retro-orbital venous plexus. Three days before and 2 weeks after the BM transplantation, recipient mice received autoclaved acidified (pH 2.7) water supplemented with 100 μg/mL neomycin and 10 μg/mL polymyxin B sulfate. Two weeks after BMT, all mice were given a Western Diet (TD00457, Harlan) for 16 weeks to induce atherosclerosis. Reconstitution of transplanted bone marrow was confirmed based on titers of E06-scFv secretion in plasma.

Atherosclerosis analysis

Mice exposed to HCD or WD were euthanized using 100% CO_2. Sections of spleen, kidney, and liver tissues were frozen in RNAlater solution (Ambion) for mRNA extraction or embedded in OCT (Sakura Tissue-Tek, Torrance, CA) for cryosectioning. After perfusion with 4% formalin-sucrose for 15 min, livers and hearts were removed, fixed and embedded in paraffin and serially sectioned. The aortas were dissected under a microscope and fixed in 4% formalin-sucrose, opened, flattened pinned and stained with Sudan IV, and images of the aortas were captured and quantified by analysis of the entire *en face* aorta as described[35]. Aortic root cross-sectional lesion areas were quantified using serial cross-sections taken at 100μm intervals between 100μm and 900μm beginning with the first appearance of the first leaflet of the aortic valve until the last leaflet. Mean lesion size at each 100μm section in each animal was determined by computer-assisted morphometry (Image-Pro Plus 6.3, Media Cybernetics) on serial 10μm paraffin sections. Modified van Gieson elastic stain was used to enhance the contrast between the intima and surrounding tissue. Cross-sectional plaque area and plaque morphology were evaluated by two investigators blinded to the study protocol. The results are presented as mean of all values for each interval plotted vs. distance from first leaflet and the overall extent of aortic root lesions was determined by area under the curve (AUC) analysis of all serial sections in each group.

In lesions of the 4-month HCD experiments, we also determined the area of necrosis by computer-assisted morphometric analysis of extent of necrosis of 5 lesions taken at each 100 μm interval and expressed as the absolute area involved at that site. In the 7-month experiment, lesions on each of the 100μm sections were selected to be of equal total size between the *Ldlr*$^{-/-}$ and *Ldlr*$^{-/-}$/E06-scFv aortic sections at that level, and the area of necrosis determined and plotted at each 100μm section. For both the 4-month and 7-month analyses, the extent of necrotic area was determined as the AUC analysis of all serial sections in each group.

Echocardiographic and histological analysis of aortic valve

Ldlr$^{-/-}$ (n =13) and *Ldlr*$^{-/-}$/E06-scFv (n =10) mice were fed a HCD for 15 months and aortic valve (AV) function was serially evaluated with Doppler ultrasound, 2D and M-mode echocardiography at 6, 9 and 12 months. At 15 months, the extent of atherosclerosis was

determined and AVs evaluated histologically. A Kaplan-Meier survival analysis was also performed on the entire cohort. Severity of aortic sclerosis was determined quantitatively by calculating peak pressure gradients across the AV using Doppler analysis and measurement of AV leaflet thickness using M-mode echocardiography. Pressure gradients were determined from aortic blood flow velocities (V) using the principles of conservation of energy and calculated by the modified Bernoulli equation [$\Delta P=4(V_{aorta}^2 - V_{LVOT}^2)$[9]. Images were acquired using high-resolution (32-55MHz) ultrasound (VisualSonics Vevo 2100) as described in Cowling et al[36]. Histological assessment of AV was determined on serial sections at 100μm intervals from the origins of the AV leaflets at the base of the aortic root, and stained for calcium using Von Kossa's method. Calcium on each section was quantified by number of pixels "stained" using Image J software. Total AV calcium was determined by area under the curve (AUC) analysis of all serial sections in each group.

Immunohistologic analyses of atherosclerotic lesions and liver tissues

Immunohistochemical studies were performed on sections of paraformaldehyde-fixed and paraffin-embedded tissues. Paraffin sections of atherosclerotic lesions, aortic roots and liver tissues were stained for OxPL with biotinylated E06 IgM, or with E06-scFv using a biotinylated mAb anti-Myc tag (Miltenyi Biotech) following the manufacturer's instruction. Endogenous peroxidase activity was blocked with 0.3% hydrogen peroxide in PBS for 15 min. After blocking, nonspecific binding sites with 10% normal goat serum and Fc Block (2.4G2 antibody) in PBS for 30 min, slides were incubated with primary antibodies for 1 h at room temperature. Biotinylated antibodies (E06, anti-myc and anti-polyHis) were revealed with ABC-HRP VectaStain kit (Vector Laboratories, Burlingame, California) and/or NovaRed substrate (Vector Labs). Slides were counterstained by hematoxylin and in some experiments, percentage of positively stained targets were quantified by image analysis morphometry (Image-Pro Plus).

Determination of cellular composition of aorta

Cellular composition of aortas was determined in the Cell Phenotyping Core of the UCSD PPG on Role of Immune Mechanisms in Inflammation and Atherosclerosis, under the direction of K. Ley, using established techniques[37]. In brief, 6 aortas from 16-week chow-fed *Ldlr*$^{-/-}$, 6 from HFD-fed *Ldlr*$^{-/-}$ and 5 from *Ldlr*$^{-/-}$Æ06-scFv mice were dissected following heparin PBS perfusion and adventitia carefully removed. The intact aortas were incubated for one hour with an Aorta Dissociation Enzyme stock solution and single cell suspensions prepared from the digested aorta by shearing the aortas apart and passing cells through a 70μm cell strainer into 5ml polypropylene FACS tubes (BD Falcon). The cells were pelleted by centrifugation (400×g, 5 minutes, 4°C), resuspended in 1ml of FACS buffer (PBS supplemented with 1% BSA and 0.05% NaN_3), counted and assessed for viability using trypan blue in a hemocytometer. Cells were stained on ice for 30 min with the panel of antibodies below, washed twice with FACS buffer and then analyzed at La Jolla Institute for Allergy and Immunology using a FACSAria analyzer. Anti-CD45 antibody and fixable live-dead cell stain (Invitrogen, Molecular Probes) was added to all samples to allow for gating of live CD45+ leukocytes and cells were sorted with the panel of antibodies listed in Table in Supplemental Information.

Analysis of T cells in blood, spleen and periaortic lymph nodes by flow cytometry

Blood from *Ldlr*$^{-/-}$ or *Ldlr*$^{-/-}$/E06-scFv mice was collected in 4% sodium citrate solution. Blood lymphocytes were obtained from the interface after underlying and spinning the blood with Histopaque 1077 (Sigma, Saint Louis, MO). Peri-aortic lymph nodes and spleens were processed to obtain single cell suspensions. Spleen samples were lysed with 1× RBC lysis buffer (BioLegend, San Diego, CA). Cell suspensions were counted using a Z2 Coulter counter (Beckman Coulter, Brea, CA) to obtain absolute numbers of each cell population. Single cell suspensions were stained as routinely done in our laboratory[38], with antibodies against CD4 (clone RM4-5; Life Technologies, Carlsbad, CA), CD8 (clone 53-6.7; Biolegend, San Diego, CA), TCRβ (peri-aortic LNs and spleen only) (clone H57-597; ebioscience, San Diego, CA), CD44 (clone IM7, Biolegend), CD25 (clone PC61, Biolegend) and live dead exclusion yellow dye (Life Technologies) in FACS buffer (2% BSA in PBS). Cells were stained on ice for 30 min, washed twice with FACS buffer and then samples were analyzed using LSRII (BD Bioscience, San Diego, CA). Data were analyzed using FlowJo 9.7 (Tree Star Inc., Ashland, OR).

RNA analysis of tissues

Total RNAs were extracted from individual frozen tissue samples (Livers) or thioglycollate elicited peritoneal macrophages (TGEM) using RNeasy mini kit (Qiagen) as per the manufacturer's instructions. Tissues were homogenized in RNeasy lysis buffer with a motorized homogenizer. Genomic DNA was removed by DNase I, and RNA concentration and quality were assessed with by NanoDrop. Next, 1 μg of RNA was reversely transcribed to cDNA using EcoDry Premix kit (Clontech). Real-time qPCR was carried out to determine gene expression of inflammatory molecules. All reactions were performed in the Rotor-Gene Q cycler (Qiagen) in triplicates using 50 ng of cDNA and qPCR Master Mix (Eurogentec, San Diego, CA), primers and Taqman fluorescent probes (Applied Biosystems) in a total reaction volume of 20 μL. Relative quantities of mRNA were calculated using ΔΔCt formula and two standard curves relative quantitation using Rotor-Gene Q Software 1.7 (Qiagen) with GAPDH as the reference gene.

Analyses of Peritoneal Macrophages

Thioglycollate-elicited peritoneal macrophages (TEM) from *Ldlr*$^{-/-}$ and *Ldlr*$^{-/-}$/E06-scFv-Tg mice fed a HCD diet for 5 weeks were isolated 3 days after intraperitoneal (i.p.) injection of 1 ml of 2% thioglycollate broth (Sigma-Aldrich) as described[13]. TGEM macrophages were collected for RNA-seq analysis, cholesterol analysis and mass spectrometry determinations of sterols as described[18]. TGEM were isolated from 3 mice in each group and each set of macrophages divided into 2 separate aliquots, which were individually extracted and sterols determined in triplicate by liquid chromatography-mass spectrometry (LC-MS/MS) following LipidMaps protocols online at www.lipidmaps.org.

In other studies to assess the ability of macrophages to secrete the E06-scFv, TGEM were obtained from E06-scFv-Tg mice plated at a density of 5 million cells/well in 6-well plates in 10% FBS in RPMI. On day 4, cells were incubated with T0901317 at 10uM/ml (or vehicle) in 1% delipidated, charcoal-stripped FBS in RPMI. Cell culture supernatants were

concentrated and assessed for E06-scFv binding activity by ELISA. Cell pellets were checked for expression of E06-scFv by qPCR.

RNA-seq analysis was performed on TGEM macrophages from 4 biological replicates. Total RNAs were converted into cDNA libraries as templates for high throughput sequencing using the Illumina HiScanSQ following the Illumina TruSeq RNA sample preparation protocol. Shortly, first strand cDNA was synthesized from 5 μg of total RNA using oligo-dT primer and EcoDry Premix kit (Clontech) for cDNA synthesis, and subsequently converted into blunt ends via exonuclease/polymerase. After adenylation of 3′ ends of DNA fragments, Illumina PE adapters were ligated to prepare cDNA fragments of preferentially 200 bp in length and enriched using Illumina PCR primers in a 15-cycle PCR reaction. After cluster generation, 100 bp paired-end reads were generated and analyzed by alignment to the UCSC murine reference genome using TopHat/Bowtie. The numbers of reads mapping to exonic and intronic regions as well as to splice sites were calculated based on the UCSC annotation file. Reads per kilobase of exon model per million mapped reads (RPKM) values for Refseq genes were established. RNA-seq clusters were analyzed by Cuffdiff2, TreeView6, for heat map, and DAVID6.7 to determine differential gene expression (DEG) between *Ldlr*$^{-/-}$ and *Ldlr*$^{-/-}$/E06-scFv macrophages, and by Gene Ontology (GO) classification to assign gene changes to different functional categories. For statistical analysis of DEG, the Cufflinks data of p-value from the t-test of RPKM in RNAseq data were further analyzed using R packages (DEseq2) from Illumina BaseSpace Sequence Hub and converted to FDR-adjusted q-values. The concise output files included only those transcripts which have a q-value lower than the given FDR, and the value of the significant-column was adjusted accordingly (yes/no) in all output files. All DEG values shown are FDR-corrected p vales < 0.05.

Determination of uptake of fluorescent OxLDL by peritoneal macrophages *in vivo*

Rag1$^{-/-}$ mice lack T and B cells and plasma antibodies. *Rag1*$^{-/-}$ *Ldlr*$^{-/-}$ mice and *Rag1*$^{-/-}$/*Ldlr*$^{-/-}$ E06-scFv transgenic mice (which only have E06-scFv Abs) were injected i.p. with 1 ml of sterile 2% thioglycollate to induce sterile peritonitis. Four days later, the mice were injected i.p. with 100μg of Alexa Fluor 488 labeled OxLDL in 200 μL PBS per mouse *Ldlr*$^{-/-}$[39]. The mice were euthanized 1hr after injection, and peritoneal cells were recovered by lavage with 10 ml of ice-cold PBS containing 1% heat-inactivated FBS and 10 mM EDTA. Peritoneal macrophages were labeled with anti-F4/80 APC conjugated mAb (eBioscience) and macrophage-specific uptake of OxLDL was analyzed by FACS for the presence of intracellular labeled OxLDL. In a separate experiment, Alexa Fluor 488 labeled OxLDL was pre-incubated with plasma from each of *Ldlr*$^{-/-}$ or *Rag1*$^{-/-}$ *Ldlr*$^{-/-}$ or *Rag1*$^{-/-}$/*Ldlr*$^{-/-}$/E06-scFv mice for 1 hour, and then injected i.p. into *Ldlr*$^{-/-}$*Rag1*$^{-/-}$ mice. In both experiments, uptake of OxLDL by elicited peritoneal macrophages *in vivo* was expressed as the percentage of macrophages ingesting OxLDL.

Statistical analysis

Unless otherwise noted, data are expressed as mean ± SEM. Statistical analysis was performed by GraphPad Prism 7.04 using the two-tailed Student's t-test and one-way ANOVA with appropriate post-hoc tests as needed. When variances were different,

differences between groups were analyzed using a nonparametric multiple comparison test. Lesion size, lesion morphology and gene expression were evaluated using the Mann–Whitney test.

Data Availability

The datasets generated during and/or analyzed during the current study are available from the corresponding author on reasonable request. The raw sequence data presented in this article have been submitted to the National Center for Biotechnology Information Sequence Read Archive (https://www.ncbi.nlm.nih.gov/sra/, BioProject) under accession number PRJNA438959.

Extended Data

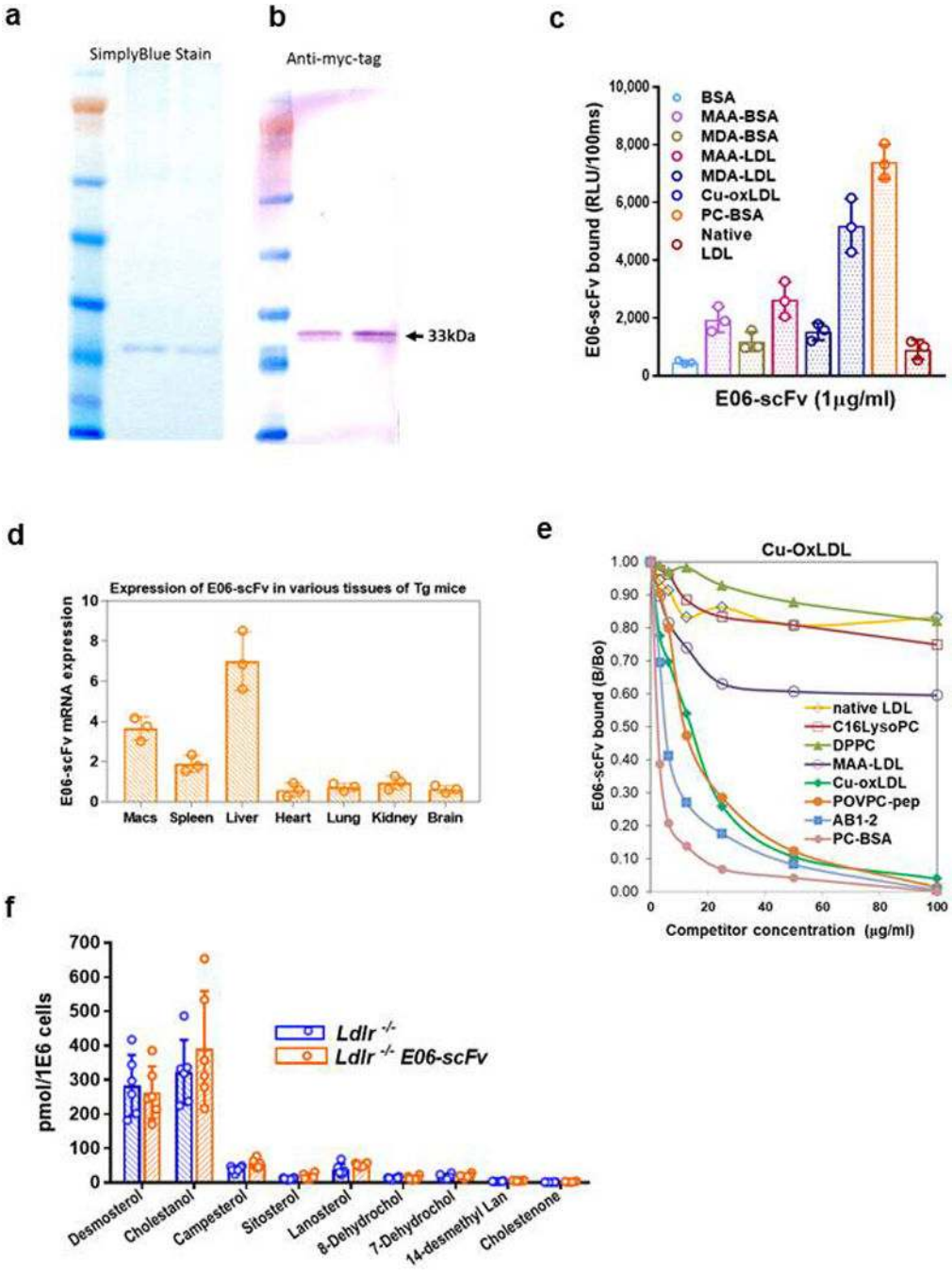

Extended Data Figure 1. E06-scFv expression and binding characteristics

a. Simply Blue staining of purified EO6-scFv from HEK293 cell lysates from two experiments. **b.** Western blot with anti-Myc of E06-scFv following purification on Ni-NTA agarose beads (representative of 4 independent experiments). **c.** Binding profile of purified E06-scFv using chemiluminescent ELISA (Binding data are mean ±SEM, using 3 independent samples, each determined in triplicate). **d**. Tissue distribution of E06-scFv gene

transcript in *Ldlr*$^{-/-}$Æ06-scFv mice determined by qPCR. (Data are mean ±SEM, determined from tissues of 3 *Ldlr*$^{-/-}$Æ06-scFv mice. **e.** Competition immunoassays of *Ldlr*$^{-/-}$Æ06-scFv plasma binding to plated OxLDL in the presence or absence of increasing amounts of indicated competitors. Results are ratio of binding of E06-scFv to OxLDL in the presence (B) or absence of competitor (B_0). AB1-2 is a T15 anti-idiotypic antibody; C16lysoPC: C16 lyso-phosphatidylcholine, DPPC: Dipalmitoyl phosphatidylcholine. Data shown are triplicates of each point from one competition experiment, representative of 4 separate studies of similar nature. **f**, Accumulation of desmosterol and other indicated sterols in TGEM from indicated mice fed a HC diet for 16 wks. TGEM were isolated from 3 mice in each group and each set of macrophages divided into 2 separate aliquots for analysis in triplicate. Data are mean ±SEM. There were no differences between respective sterol pairs, $p>0.05$ for all pairs.

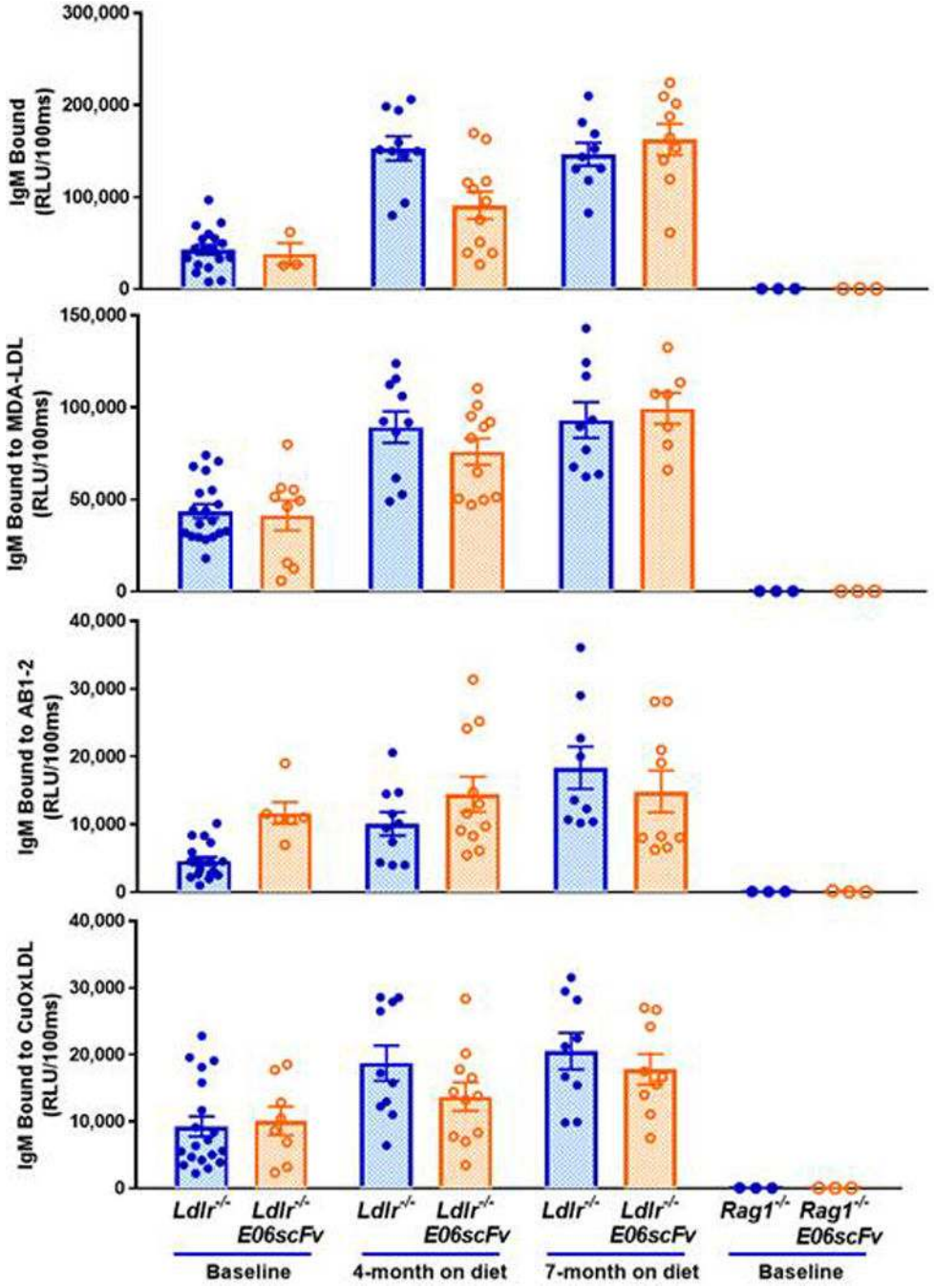

Extended Data Figure 2. Expressed E06-scFv does not alter levels of total IgM or IgM E06 (detected by AB1-2) in transgenic mice

Comparison of plasma IgM titers to indicated antigens of *Ldlr*$^{-/-}$or *Ldlr*$^{-/-}$Æ06-scFv mice at baseline or after 4 or 7 months of HC diets. Note significant increases in Total IgM and IgM to MDA-LDL and OxLDL at 4 and 7 months vs. respective baseline titers (all vales $p < 0.001$) except at 4 months, total IgM of *Ldlr*$^{-/-}$Æ06-scFv mice and E06 (detected by AB1-2) in both mouse groups were not different than their respective baselines ($p > 0.05$). Importantly, there were no significant differences in any antibody titers between *Ldlr*$^{-/-}$ *or* *Ldlr*$^{-/-}$Æ06-scFv mice at any time point, and in particular, note that endogenous IgM-E06

titers (detected by AB1-2 binding) were similar. As expected, the *Rag1*$^{-/-}$ and Rag$^{-/-}$/E06-sc did not have any IgM.

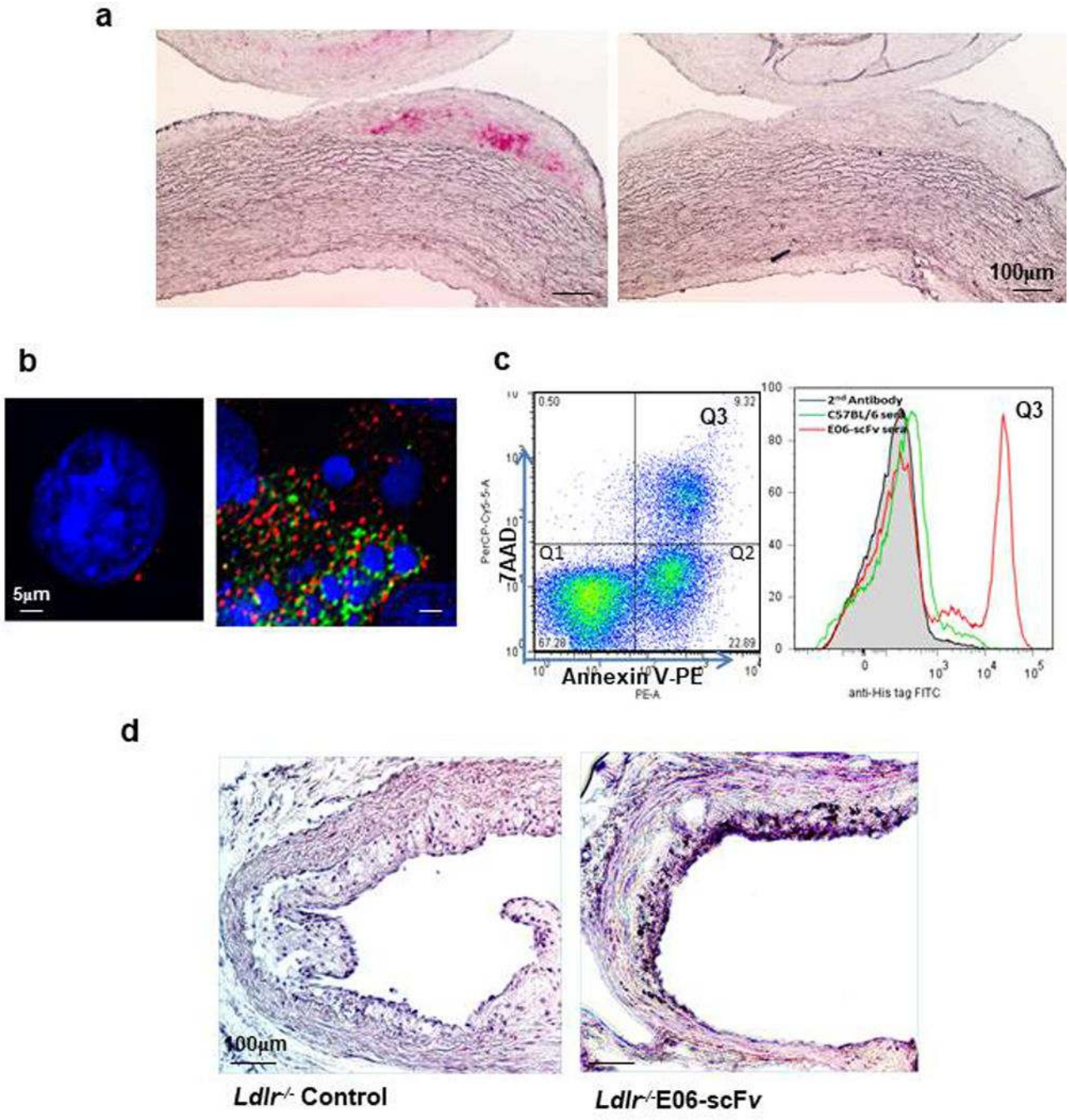

Extended Data Figure 3. Plasma E06-scFv binds to atherosclerotic lesions and apoptotic thymocytes and is present in aorta of *Ldlr*$^{-/-}$/E06-scFv mice

a, Staining of atherosclerotic lesions of WHHL rabbit aorta with E06-scFv plasma (left panel), and *Ldlr*$^{-/-}$ mice (right panel) (both at dilution of 1:20), visualized using biotinylated anti-Myc mAb and ABC-AP VectaStain kit. **b**, Deconvolution microscopy of E06-scFv plasma (1:20 dilution) binding to apoptotic but not normal cells. Blue, nuclei stained with

Hoechst dye; Green, FITC-labeled anti-His tag mAb; Red, Annexin V-PE. **c**, Binding of E06-scFv plasma (1:20 dilution) to apoptotic thymocytes (7AAD+/Annexin V+) by FACS analysis. **d**, Expression of E06-scFv in aortic lesion of *Ldlr*$^{-/-}$Æ06-scFv but not *Ldlr*$^{-/-}$ mouse. Cross-sections at the AV were stained with biotinylated anti-Myc mAb to identify presence of E06-scFv in atherosclerotic lesion. Nuclei counterstained using Hematoxylin QS (Original ×200). Panels a-c are representative of similar studies with 5 other plasma samples. Panel d is representative of studies in 3 other aortic sections.

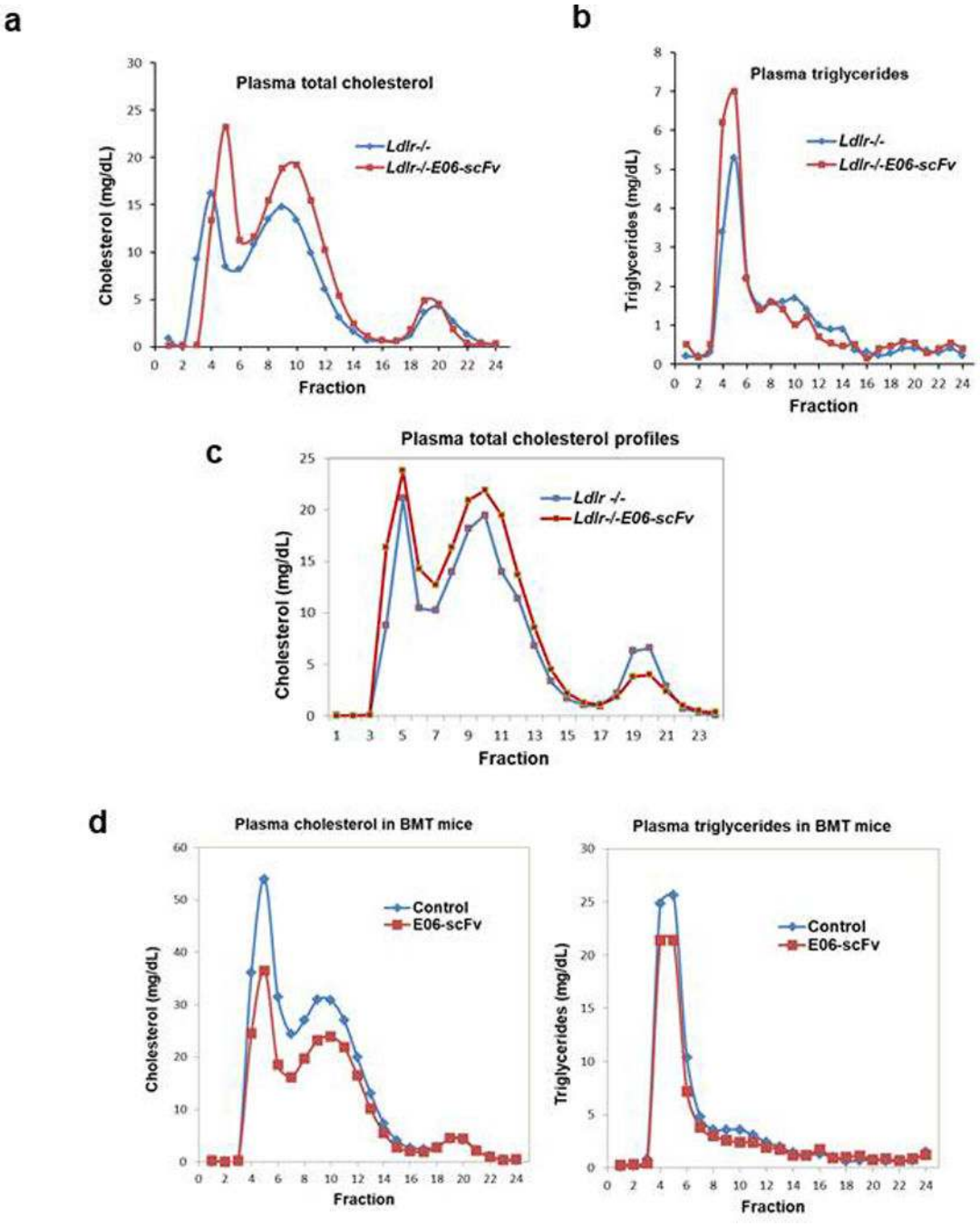

Extended Data Figure 4. Lipoprotein profiles of *Ldlr*$^{-/-}$ *and Ldlr*$^{-/-}$/E06-scFv mice are similar in various studies

a, b, Plasma cholesterol (a), and triglycerides (b) distribution by FPLC in pools of equal aliquots of plasma from mice fed HC diet for 16 weeks (n=10, 11). **c**, Plasma cholesterol distribution in mice fed HC diet for 28 weeks (n=9,7). **d**, Plasma cholesterol and triglyceride distribution in BMT experiment: Lipoprotein profiles in *Ldlr*$^{-/-}$ mice that received BM from wild type (control, n=9) or E06-scFv mice (n=13) and then fed a WD for 16 weeks.

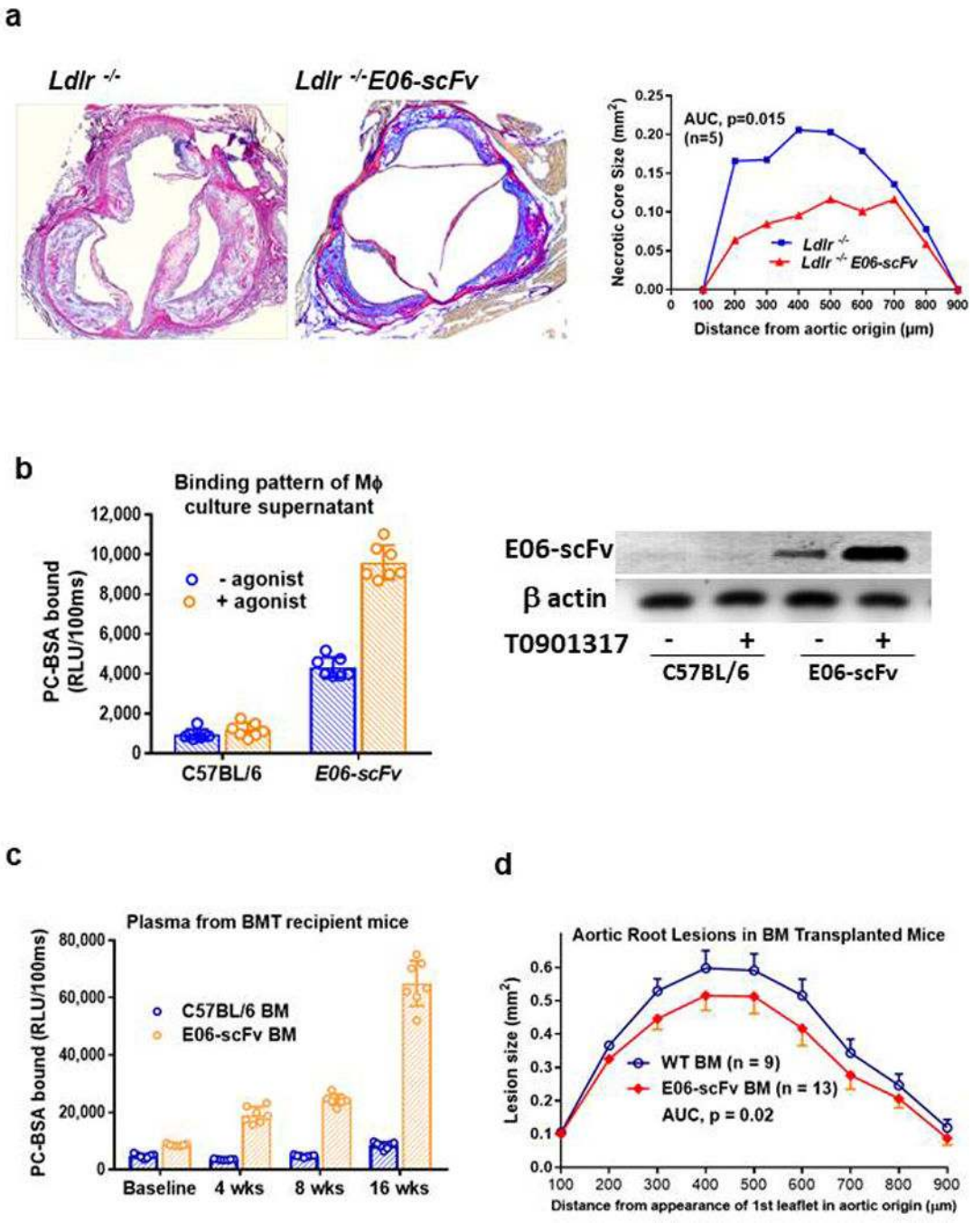

Extended Data Figure 5. E06-scFv reduces necrotic core formation and macrophage secretion of E06-scFv confers atheroprotection

a, E06-scFv reduces extent of necrosis within aortic root lesions after HCD for 7 months as shown in Fig 2c. Lesions of equal size were matched at each of the indicated sites in aortic root sections from 7 *Ldlr*$^{-/-}$ *and 9 Ldlr*$^{-/-}$*/*E06-scFv mice and extent of necrosis measured as described in Methods. Necrosis was reduced by 43.9% in *Ldlr*$^{-/-}$*/*E06-scFv mice (AUC 113.4 vs. 63.6, p=0.015). **b**, Secretion of E06-scFv in cultured peritoneal macrophages in the absence or presence of LXR agonist T090137 from C57BL/6 (WT) and E06-scFv mice determined by PC-binding assay. Culture supernatants were concentrated 10-fold for ELISA (left panel). The E06-scFv expression, driven by the *apoE* promoter was stimulated by T0901317 as indicated by Western blots of cell lysates with anti-myc mAb (right panel). Representative of 4 separate experiments. **c**, Plasma E06-scFv titers following transplantation (baseline) in *Ldlr*$^{-/-}$ mice transplanted with WT (n=7) or E06-scFv (n=7) bone marrow). E06-scFv titers (plasma from 7 WT and 7 E06-scFv) increased in mice transplanted with E06-scFv BM over 16 weeks of WD. **d**, Aortic root atherosclerosis in *Ldlr* $^{-/-}$ mice transplanted with WT (n=9) or E06-scFv (n=13) bone marrow after 16 weeks of WD. As described in Methods, aortic root lesion areas were quantified from serial sections (9 sections per mouse) cut through the aorta at the origins of the AV leaflets and then stained with modified van Geison solution. Lesions at aortic root were reduced by 37% in mice that received BMT from E06-scFv mice (AUC 69.6 vs 110.6, p=0.02, two-sided-t-test).

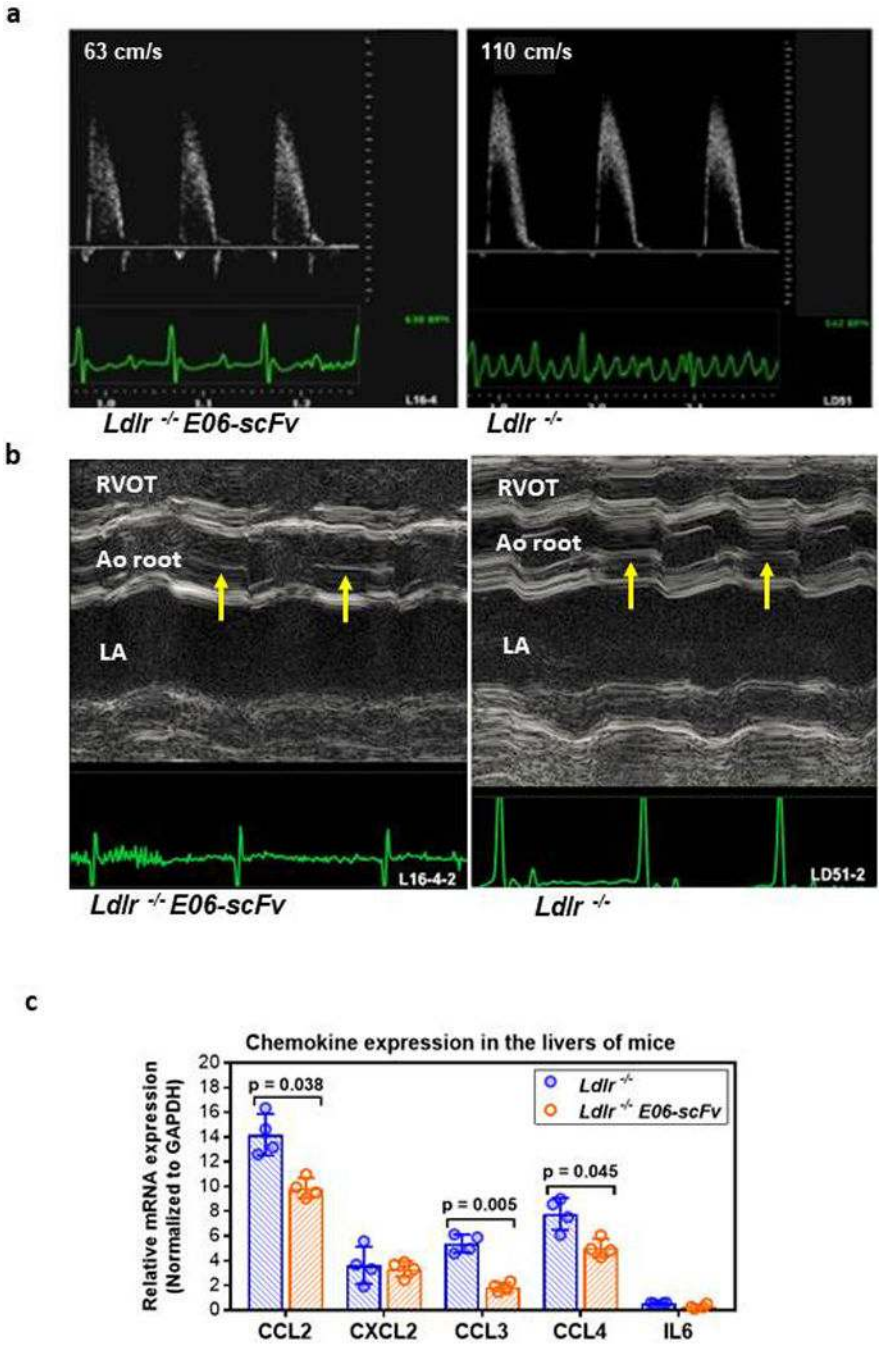

Extended Data Figure 6. AV echocardiography and hepatic gene Expression

a Representative pulse wave Doppler derived aortic jet velocities in 12 month old *Ldlr*$^{-/-}$/E06-scFv (left) and *Ldlr*$^{-/-}$ (right) mouse: ECG tracings are shown in green. Representative of studies in 9 *Ldlr*$^{-/-}$ and 10 *Ldlr*$^{-/-}$/E06-scFv mice. **b.** Representative M-mode echocardiography images containing the AV in short axis through the right ventricular outflow tract (RVOT), aortic (Ao) root with AV, and left atrium (LA). The AV (arrows), best observed in diastole, is thinner in *Ldlr*$^{-/-}$/E06-scFv compared to *Ldlr*$^{-/-}$ mice. ECG tracings shown in green. Representative of studies in 9 *Ldlr*$^{-/-}$ and 10 *Ldlr*$^{-/-}$/E06-scFv mice. c.

Decreased inflammatory gene expression in whole liver extracts of *Ldlr*$^{-/-}$ and *Ldlr*$^{-/-}$/E06-scFv mice after 16 weeks of HC diet. Relative mRNA levels were determined by qPCR and normalized to GAPDH and expressed as means ± SEM. (n=4 mice each).

Extended Data Table 1
Weights and lipid levels in mice in atherogenic studies

a. Indicated parameters for mice on the HCD diets for 4, 7 or 12 month studies. Results represent the mean ± SEM. For mice on the 4 month diet protocol, plasma cholesterol and triglyceride were measured at baseline, 4 wks, 8 wks and at 4 months. For mice in the 7 and 12 months protocols, measurements were made at time of sacrifice. There were no significant differences between mice at any given time point. (For the 4, 7 and 12 month protocols, *Ldlr*$^{-/-}$ (n = 10, 9, 8) and *Ldlr*$^{-/-}$/E06-scFv (n =11, 7, 10 respectively). **b.** Variables at indicated times in *Ldlr*$^{-/-}$ recipient mice on the WD following BM transplantation from C57BL/6 or E06-scFv mice on C57BL/6 background. Results represent the mean ± SEM. There are no significant differences between mice at any given time point. (Number of mice for C57BL/6 donors, n = 9; for E06-scFv donors, n = 13).

a

Time Course Groups	-2 weeks (Baseline)		4 weeks		8 weeks		4 months		7 months	
	Ldlr$^{-/-}$	E06-scFv	*Ldlr*$^{-/-}$	06-scFv	*Ldlr*$^{-/-}$	E06-scFv	*Ldlr*$^{-/-}$	E06-scFv	*Ldlr*$^{-/-}$	E06-scFv
Weight (g) ± SEM	25.1±0.5	22±1.1	27.5±0.5	24±1.1	28.2±0.5	24.9±1.1	30.7±0.6	26.7±1.3	35.2±4.2	34.8±3.6
Total Chol (mg/dL)	269±9.5	246±9.9	944±63	957±52	852±55	925±46	624±38	881±125	790±240	937±135
Triglyceride (mg/dL)	88±9.2	139±9.7	135±12	141±17	111±7.5	123±12	128±7.7	151±14	161±54	199±78

b

Time Course Groups	–2 weeks (Baseline)		4 weeks		8 weeks (Midpoint)		16 weeks (Endpoint)	
	C57BL	E06-scFv	C57BL	E06-scFv	C57BL	E06-scFv	C57BL	E06-scFv
Weight (g) ± SEM	22.3±1.6	23.4±2.4	24.5±1.7	25±2.4	26.2±0.7	26.1±2.9	26.8±1.7	27.4±2.4
Total Chol (mg/dL)	248±23	240±25	1231±64	1328±95	1444±140	1240±143	1579±168	1215±216
Triglyceride (mg/dL)	92±16	112±30	176±50	202±53	143±25	178±44	578±83	433±62

Extended Data Table 2
GO analysis of differentially expressed genes in macrophages of *Ldlr*$^{-/-}$ and *Ldlr*$^{-/-}$/E06-scFv mice

GO analysis of genes that were increased >1.5 fold in TGEM of *Ldlr*$^{-/-}$/E06-scFv mice compared to *Ldlr*$^{-/-}$ mice. Experimental details and major gene changes shown in Figure 3. Data of TGEM from 4 mice each group.

Go Analysis: Genes Expression >1.5 fold higher in E06-scFv Transgenic Mice			
Term	**Count**	**%**	**P-value**
GO:0006955 ~ immune response	45	16.4234	9.37E-26
GO:0009615 ~ response to virus	12	4.3796	3.69E-09

Go Analysis: Genes Expression >1.5 fold higher in E06-scFv Transgenic Mice			
Term	**Count**	**%**	**P-value**
GO:0002684 ~ positive regulation of immune system process	17	6.2044	1.12E-08
GO:0045087 ~ innate immune response	13	4.7445	1.39E-08
GO:0006952 ~ defense response	24	8.7591	1.89E-08
GO:0050778 ~ positive regulation of immune response	14	5.1095	2.40E-08
GO:0002460 ~ adaptive immune response based on somatic recombination of immune receptors built from immunoglobulin superfamily domains	11	4.0146	1.31E-07
GO:0002250 ~ adaptive immune response	11	4.0146	1.31E-07

Extended Data Table 3

Cell counts of viable aortic cells determined from FACS analysis

Cell counts of viable aortic cells isolated from aortas of chow-fed and HCD-fed *Ldlr*$^{-/-}$ mice and HCD-fed *Ldlr*$^{-/-}$/E06-scFv mice. Values are mean ± SD of total viable cells evaluated by flow cytometry per aorta as described in methods. Number of aorta for each group: HCD-*Ldlr*$^{-/-}$/E06-scFv = 5; Chow-*Ldlr*$^{-/-}$ = 6; and HCD-*Ldlr*$^{-/-}$ = 6.

Group	Total Viable cells*	Monocytes (% of Total)	Lymphocytes (% of Total)	B cells (% of Lymph	T cells (% of Lymph)
HCD *E06-scFv*	3398±2615	43±7.1	57±7.1	4.1±2.0	54±11
Chow- *Ldlr*$^{-/-}$	864±1085	43±15	57±15	7.5±5.1	29±15
HCD– *Ldlr*$^{-/-}$	7829**±10.247	18±4.6	82±4.6	12±20	62±15

*Note that one aorta in the HCD-*Ldlr*$^{-/-}$ had extensive atherosclerosis and had 27,846 viable cells counted. The next highest value in this group was 9,342; By comparison, the highest in the Chow-*Ldlr*$^{-/-}$ group was 2909 and in the HCD-*Ldlr*$^{-/-}$/E06-scFv group was 5692. Aortic cells were evaluated by flow cytometry as described in Methods. Data for phenotype of monocyte/macrophages are shown in Figure 3.

Extended Data Table 4

Echocardiographic parameters of mice after 12 months of HCD

Values are mean±SD and p values refer to comparisons of – *Ldlr*$^{-/-}$ vs *Ldlr*$^{-/-}$/E06-scFv mice using two-sided-t-test. FS, fractional shortening; HR, heart rate; IVSD, interventricular septum during diastole; LVIDd, left ventricular internal diameter during diastole; LVIDs, left ventricular internal diameter during systole; LVPWd, left ventricular posterior wall thickness during diastole; LVM/BW, ratio of left ventricle mass to body weight. This table includes studies in 2 *Ldlr*$^{-/-}$ mice not included in Fig 4a.

Parameters	*Ldlr*$^{-/-}$ (n=13)	*Ldlr*$^{-/-}$ *E06-scFv* (n=10)	P value
HR (bpm)	528±55	562±51	0.18
IVSd (mm)	0.75±0.08	0.73±0.05	0.55
LVIDd(mm)	3.68±0.45	3.76±0.39	0.67
LVIDs(mm)	2.51±0.42	2.60±0.43	0.63
LVPWd(mm)	0.73±0.08	0.71±0.07	0.54

Parameters	*Ldlr*$^{-/-}$ (n=13)	*Ldlr*$^{-/-}$ *E06-scFv* (n=10)	P value
%FS	31.8±7.3	31.0±7.9	0.78
LVM/BW Aortic Valve	25.2±5.0	25.6±4.1	0.84
–Peak Velocity (cm/s)	103.22±28.23	79.25±29.50	0.020
–Peak Gradient (mmHg)	4.56±2.43	2.83±1.91	0.025

Supplementary Material

Refer to Web version on PubMed Central for supplementary material.

Acknowledgments

This work was supported by NIH Grants: HL088093 (X.Q., S.T., C.K.G., K.L., Y.I.M., J.L.W.), HL086559 (J.L.W.) HL119828 (J.L.W., S.T.), HL055798 (S.T., J.L.W., Y.I.M., K.L., C.C.H.) HL136275 (S.T., J.L.W., Y.I.M.), R35 HL135737 (J.L.W.,Y.I.M.) HL055798 and HL112276 (C.C.H.), HL20948 (J.G.M.) DRC P30 DK063491 (P.L.M.), P42 ES010337 (P.L.M.), P30 CA23100 (P.L.M.), Center for Human Nutrition grant 550015400 (J.G.M.), and Leducq Foundation Transatlantic Grants to J.L.W. and to C.K.G.. X.Q. was supported in part by a Grant-in-Aid from American Heart Association, and D.E.G. was supported in part by American Heart Association post-doctoral grant (13POST16990031).

X.Q., S.T. and J.L.W. are co-inventors and receive royalties from patents owned by the University of California San Diego on the use of oxidation-specific antibodies. S.T. currently has a dual appointment at UCSD and as an employee of Ionis Pharmaceuticals. J.L.W. is a consultant to Ionis Pharmaceuticals.

BIBLIOGRAPHY

1. Binder CJ, Papac-Milicevic N, Witztum JL. Innate sensing of oxidation-specific epitopes in health and disease. Nat Rev Immunol. 2016; 16:485–497. [PubMed: 27346802]
2. Shaw PX, et al. Natural antibodies with the T15 idiotype may act in atherosclerosis, apoptotic clearance, and protective immunity. J Clin Invest. 2000; 105:1731–1740. [PubMed: 10862788]
3. Friedman P, Horkko S, Steinberg D, Witztum JL, Dennis EA. Correlation of antiphospholipid antibody recognition with the structure of synthetic oxidized phospholipids. Importance of Schiff base formation and aldol condensation. J Biol Chem. 2002; 277:7010–7020. [PubMed: 11744722]
4. Chang MK, et al. Apoptotic cells with oxidation-specific epitopes are immunogenic and proinflammatory. J Exp Med. 2004; 200:1359–1370. [PubMed: 15583011]
5. Miller YI, et al. Oxidation-specific epitopes are danger-associated molecular patterns recognized by pattern recognition receptors of innate immunity. Circ Res. 2011; 108:235–248. [PubMed: 21252151]
6. Tsiantoulas D, et al. Circulating microparticles carry oxidation-specific epitopes and are recognized by natural IgM antibodies. J Lipid Res. 2015; 56:440–448. [PubMed: 25525116]
7. Lee S, et al. Role of phospholipid oxidation products in atherosclerosis. Circ Res. 2012; 111:778–799. [PubMed: 22935534]
8. Imai Y, et al. Identification of oxidative stress and Toll-like receptor 4 signaling as a key pathway of acute lung injury. Cell. 2008; 133:235–249. [PubMed: 18423196]
9. Baldan A, et al. ABCG1 Is Required for Pulmonary B-1 B Cell and Natural Antibody Homeostasis. J Immunol. 2014; 193:5637–5648. [PubMed: 25339664]
10. Haider L, et al. Oxidative damage in multiple sclerosis lesions. Brain. 2011; 134:1914–1924. [PubMed: 21653539]
11. Liu B, et al. Oxidized Phospholipid OxPAPC Activates TRPA1 and Contributes to Chronic Inflammatory Pain in Mice. PLoS One. 2016; 11:e0165200. [PubMed: 27812120]

12. Oehler B, et al. Inflammatory pain control by blocking oxidized phospholipid-mediated TRP channel activation. Scientific reports. 2017; 7:5447. [PubMed: 28710476]
13. Ikura Y, et al. Localization of oxidized phosphatidylcholine in nonalcoholic fatty liver disease: impact on disease progression. Hepatology. 2006; 43:506–514. [PubMed: 16496325]
14. Tsimikas S. A Test in Context: Lipoprotein(a): Diagnosis, Prognosis, Controversies, and Emerging Therapies. J Am Coll Cardiol. 2017; 69:692–711. [PubMed: 28183512]
15. Turner WW, et al. Design and synthesis of a stable oxidized phospholipid mimic with specific binding recognition for macrophage scavenger receptors. J Med Chem. 2012; 55:8178–8182. [PubMed: 22934615]
16. Seimon TA, et al. Atherogenic lipids and lipoproteins trigger CD36-TLR2-dependent apoptosis in macrophages undergoing endoplasmic reticulum stress. Cell Metab. 2010; 12:467–482. [PubMed: 21035758]
17. Laffitte BA, et al. LXRs control lipid-inducible expression of the apolipoprotein E gene in macrophages and adipocytes. Proc Natl Acad Sci U S A. 2001; 98:507–512. [PubMed: 11149950]
18. Spann NJ, et al. Regulated accumulation of desmosterol integrates macrophage lipid metabolism and inflammatory responses. Cell. 2012; 151:138–152. [PubMed: 23021221]
19. Kamstrup PR, Hung MY, Witztum JL, Tsimikas S, Nordestgaard BG. Oxidized Phospholipids and Risk of Calcific Aortic Valve Disease: The Copenhagen General Population Study. Arterioscler Thromb Vasc Biol. 2017
20. Houben T, et al. Blood-derived macrophages prone to accumulate lysosomal lipids trigger oxLDL-dependent murine hepatic inflammation. Scientific reports. 2017; 7:12550. [PubMed: 28970532]
21. Lewis KE, et al. Increase in serum amyloid a evoked by dietary cholesterol is associated with increased atherosclerosis in mice. Circulation. 2004; 110:540–545. [PubMed: 15277327]
22. Popat RJ, et al. Anti-myeloperoxidase antibodies attenuate the monocyte response to LPS and shape macrophage development. JCI insight. 2017; 2:e87379. [PubMed: 28138552]
23. Zanoni I, Tan Y, Di Gioia M, Springstead JR, Kagan JC. By Capturing Inflammatory Lipids Released from Dying Cells, the Receptor CD14 Induces Inflammasome-Dependent Phagocyte Hyperactivation. Immunity. 2017; 47:697–709 e693. [PubMed: 29045901]
24. Podrez EA, et al. Identification of a novel family of oxidized phospholipids that serve as ligands for the macrophage scavenger receptor CD36. J Biol Chem. 2002; 277:38503–38516. [PubMed: 12105195]
25. Kadl A, et al. Oxidized phospholipid-induced inflammation is mediated by Toll-like receptor 2. Free Radic Biol Med. 2011; 51:1903–1909. [PubMed: 21925592]
26. Towler DA. Molecular and cellular aspects of calcific aortic valve disease. Circ Res. 2013; 113:198–208. [PubMed: 23833294]
27. Ambrogini E, et al. Oxidation-specific Epitopes Restrain Bone Formation. Nature Comm. 2018
28. Briley-Saebo K, Yeang C, Witztum JL, Tsimikas S. Imaging of oxidation-specific epitopes with targeted nanoparticles to detect high-risk atherosclerotic lesions: progress and future directions. Journal of cardiovascular translational research. 2014; 7:719–736. [PubMed: 25297940]
29. Tsimikas S, et al. Human oxidation-specific antibodies reduce foam cell formation and atherosclerosis progression. J Am Coll Cardiol. 2011; 58:1715–1727. [PubMed: 21982317]
30. Senders ML, et al. PET/MR Imaging of Malondialdehyde-Acetaldehyde Epitopes With a Human Antibody Detects Clinically Relevant Atherothrombosis. J Am Coll Cardiol. 2018; 71:321–335. [PubMed: 29348025]
31. Gonen A, et al. Atheroprotective immunization with malondialdehyde-modified LDL is hapten specific and dependent on advanced MDA adducts: implications for development of an atheroprotective vaccine. J Lipid Res. 2014; 55:2137–2155. [PubMed: 25143462]
32. Chou MY, et al. Oxidation-specific epitopes are dominant targets of innate natural antibodies in mice and humans. J Clin Invest. 2009; 119:1335–1349. [PubMed: 19363291]
33. Schneider M, et al. High-level lipoprotein [a] expression in transgenic mice: evidence for oxidized phospholipids in lipoprotein [a] but not in low density lipoproteins. J Lipid Res. 2005; 46:769–778. [PubMed: 15654123]

34. Montano EN, et al. Development and application of a nonradioactive binding assay of oxidized low-density lipoprotein to macrophage scavenger receptors. J Lipid Res. 2013; 54:3206–3214. [PubMed: 23997238]

35. Binder CJ, et al. IL-5 links adaptive and natural immunity specific for epitopes of oxidized LDL and protects from atherosclerosis. J Clin Invest. 2004; 114:427–437. [PubMed: 15286809]

36. Cowling RT, et al. Discoidin domain receptor 2 germline gene deletion leads to altered heart structure and function in the mouse. Am J Physiol Heart Circ Physiol. 2014; 307:H773–781. [PubMed: 24993042]

37. Butcher MJ, Herre M, Ley K, Galkina E. Flow cytometry analysis of immune cells within murine aortas. Journal of visualized experiments: JoVE. 2011

38. Nowyhed HN, et al. The nuclear receptor nr4a1 controls CD8 T cell development through transcriptional suppression of runx3. Scientific reports. 2015; 5:9059. [PubMed: 25762306]

39. Choi SH, et al. Lipoprotein accumulation in macrophages via toll-like receptor-4-dependent fluid phase uptake. Circ Res. 2009; 104:1355–1363. [PubMed: 19461045]

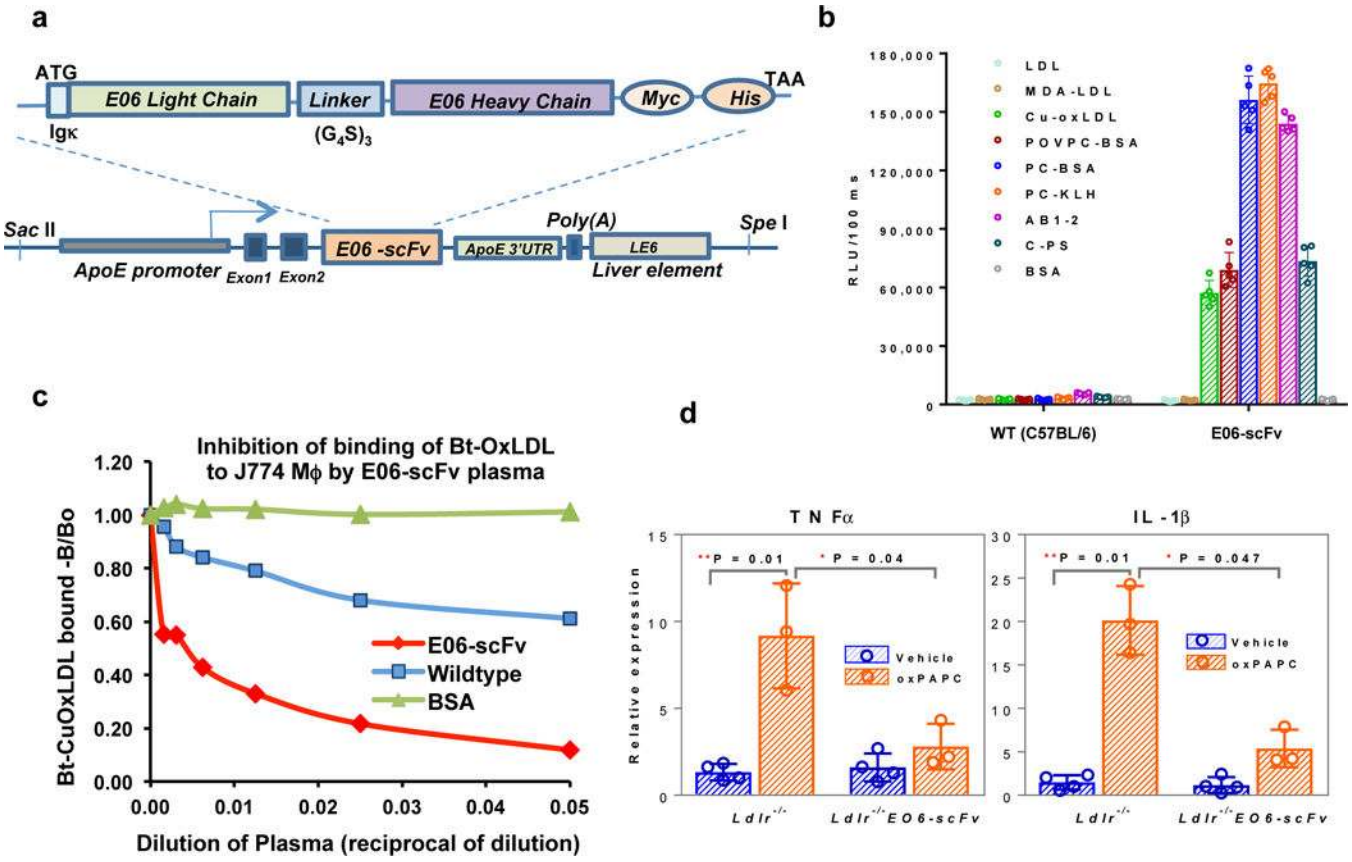

Figure 1. Transgenic mice expressing a single chain variant of E06 (E06-scFv)

a, The configuration of the E06 single-chain transgene, which encodes the E06 light and heavy chains with flexible linker (Gly4Ser)3 and epitope tags under the direction of *Apo*E promoter and LE6 enhancer. **b**, Binding properties of plasma from wild-type C57BL/6 and the E06-scFv mice to indicated antigens (mean±SEM, n=5 plasmas from each group, each point determined in triplicate). **c**, Plasma from E06-scFv mice reduced OxLDL binding by macrophages in culture. Shown is one experiment, each point in triplicate, and representative of 5 separate experiments. **d**, E06-scFv protected thioglycollate elicited peritoneal macrophages (TGEM) from OxPAPC induced inflammatory response. OxPAPC or vehicle (PBS) were injected ip into *Ldlr*$^{-/-}$ *or Ldlr*$^{-/-}$/E06-scFv mice and TGEM macrophages were collected 4h after injection for qPCR analysis. Data are mean ± SEM normalized to control; (n=3,4 mice per group).

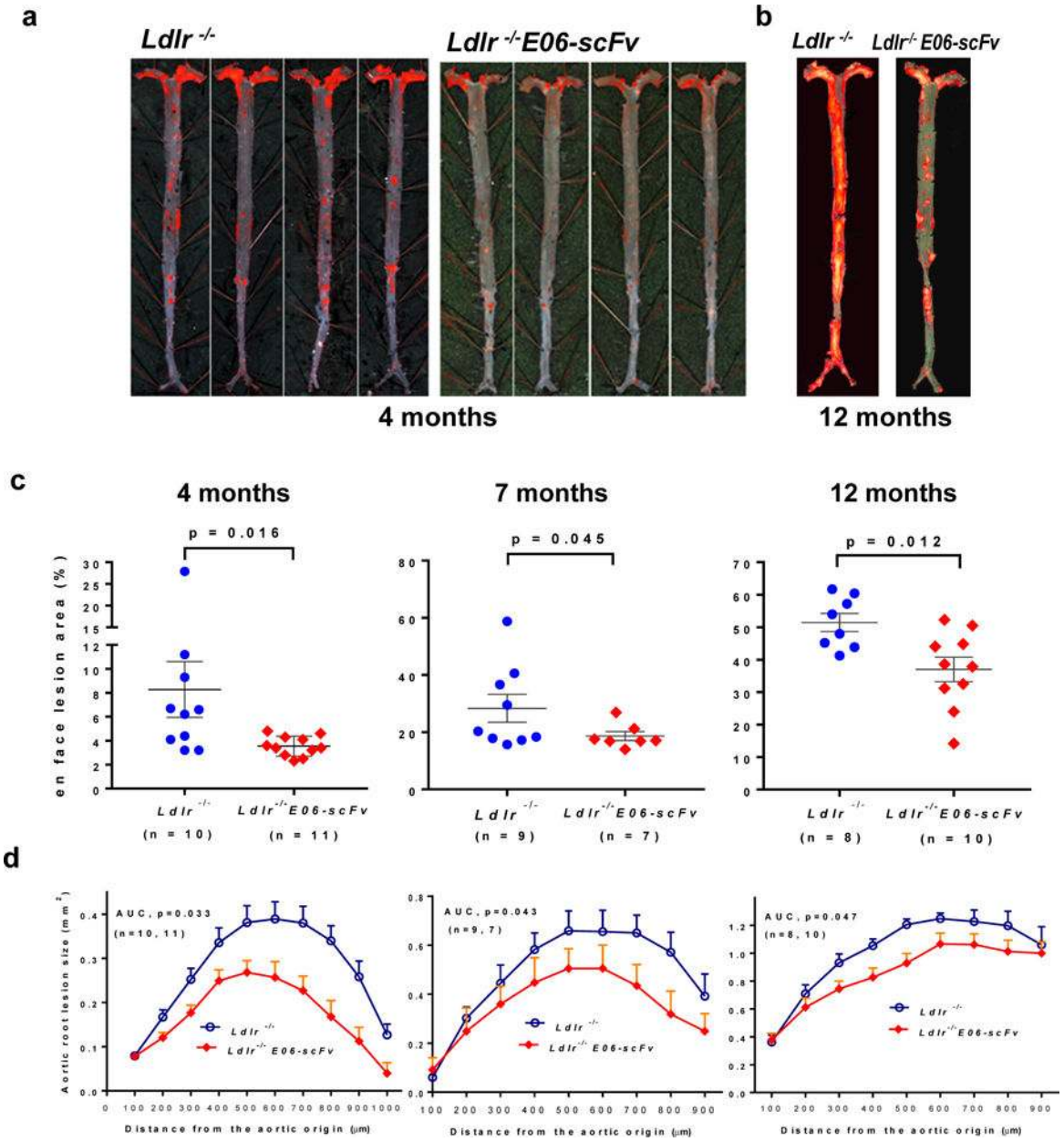

Figure 2. E06-scFv reduces atherosclerosis in HC-fed *Ldlr-/-* mice

a, b, Examples of e*n face* atherosclerosis in *Ldlr*$^{-/-}$ and *Ldlr*$^{-/-}$Æ06-scFv mice after 4 months (**a**) and 12 months (**b**) of 1% high cholesterol diet (HCD). **c, d**, Cumulative data for extent of *en face* lesion formation in the entire aorta (**c**) or at the aortic root (**d**) of *Ldlr*$^{-/-}$ (n =8-10) and *Ldlr*$^{-/-}$Æ06-scFv mice (n =7-11). Compared to *Ldlr*$^{-/-}$ mice, atherosclerosis was significantly reduced in *Ldlr*$^{-/-}$Æ06-scFv mice at 4, 7 and 12 months (*en face* by 57%, 34% and 28%, and aortic root by 55%, 41% and 27% respectively).

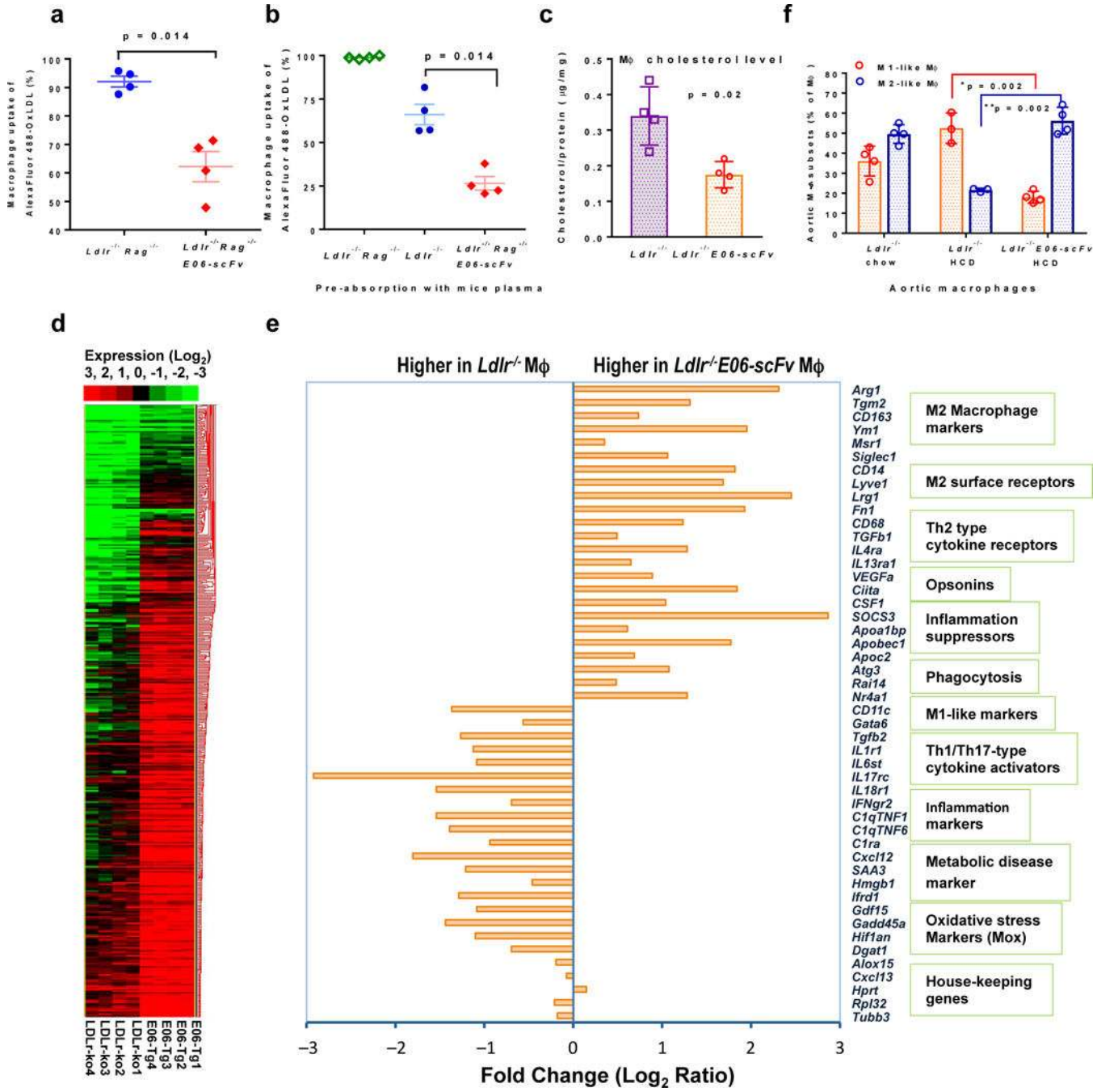

Figure 3. Mechanisms by which E06-scFv decreases atherosclerosis

a, AlexaFluor 488 labeled OxLDL was injected i.p. and macrophage uptake of OxLDL was determined by FACS and expressed as % macrophages taking up OxLDL. Macrophage uptake was reduced in *Ldlr*$^{-/-}$/*Rag1*$^{-/-}$/E06-scFv compared to *Ldlr*$^{-/-}$/*Rag1*$^{-/-}$ mice (% uptake 91±1.03 vs. 62±5.01, 4 mice each). **b**, AlexFluor labeled OxLDL was pre-incubated with plasma from *Ldlr*$^{-/-}$/*Rag1*$^{-/-}$ or *Ldlr*$^{-/-}$ or *Ldlr*$^{-/-}$/*Rag1*$^{-/-}$/E06-scFv mice, and injected into corresponding mice (n =4 each) and macrophage uptake determined as in **a**. The % of macrophages that took up OxLDL was 98.83±0.44, 66.06±5.87, and 26.48±3.90

respectively. The ~ 25% decrease observed following incubation with *Ldlr*$^{-/-}$ plasma possibly reflects the presence of endogenous anti-OxLDL antibodies. **c**, TGEM from 16 week HCD mice (n=4 mice each) were isolated and cellular cholesterol and desmosterol and other oxysterol levels determined and normalized to cellular protein. Total cholesterol accumulation shown here was reduced 48% in *Ldlr*$^{-/-}$Æ06-scFv mice (Data are mean ± SD; n = 4). Desmosterol and oxysterol levels were similar (see Extended Data Fig 1d). **d**, Heat map of RNAseq data from *Ldlr*$^{-/-}$ and *Ldlr*$^{-/-}$Æ06-scFv TGEM collected after 16 weeks of HCD (n = 4 each group). **e**, Selected list of differentially expressed transcripts in TGEM (Mϕ) based on clustering analysis on log ratio RPKM data from d. All values represent FDR-adjusted p values < 0.05 as described in Methods. **f**, Aortic wall tissue-resident macrophage phenotypes were determined by FACS analysis of CD45^{+} viable cells. Macrophages were defined as M1-like (CD11b^{+}CD11c^{+}Arg1^{-}) or M2-like (CD11b^{+}CD11c^{-}Arg1^{+}) and expressed as % Frequency of parent (CD11b^{+}CD11C$^{+/-}$) (*Ldlr*$^{-/-}$chow and *Ldlr*$^{-/-}$/E06-scFv HCD (n=4), *Ldlr*$^{-/-}$HCD (n=3).

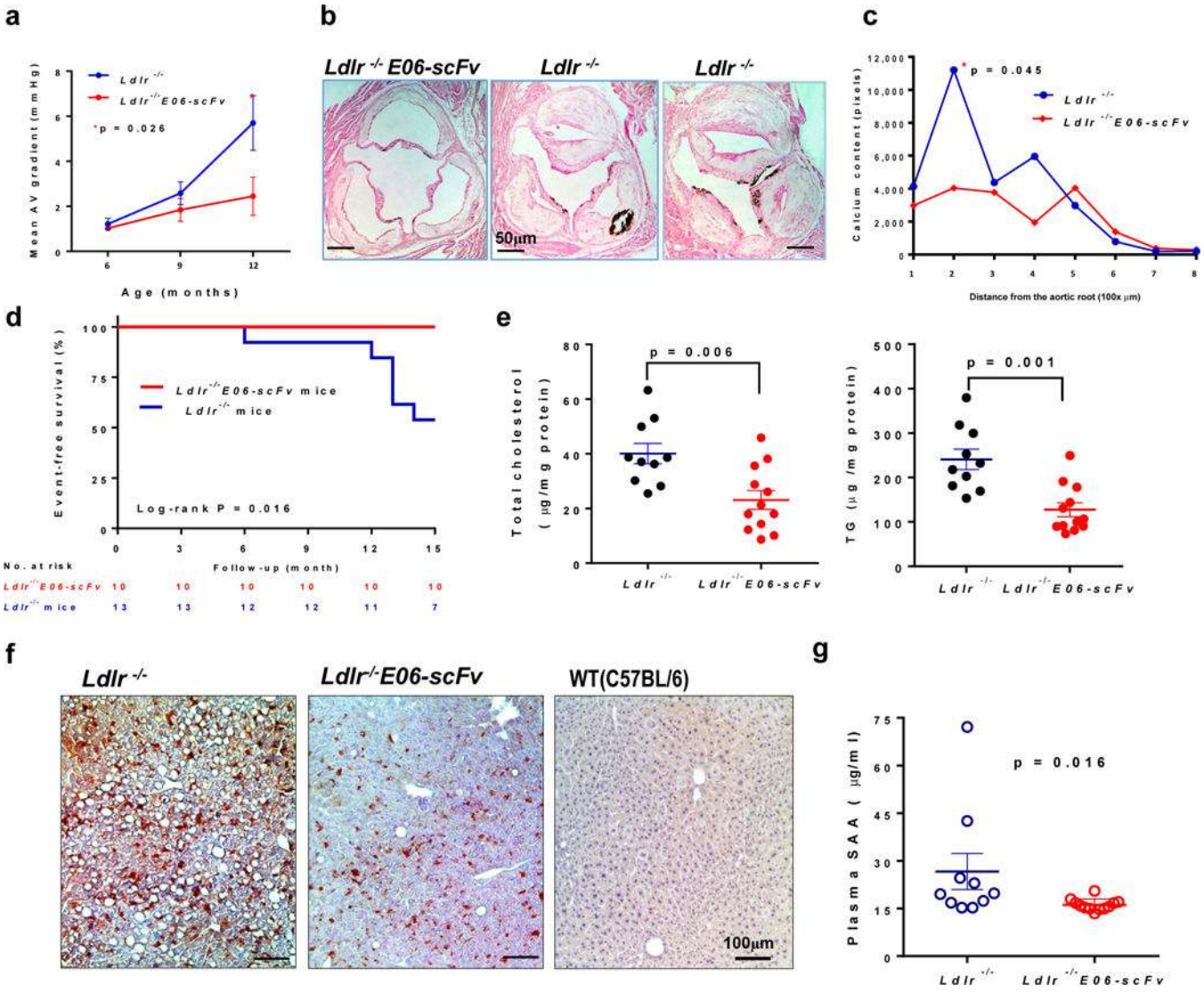

Figure 4. E06-scFv decreases early aortic valve stenosis, hepatic steatosis, and systemic inflammation

a, b, *Ldlr*$^{-/-}$ *(n=11) and Ldlr*$^{-/-}$/E06-scFv (n=10) mice were fed HCD for 15 months and prospectively examined at 3 time points for aortic valve hemodynamics. **a**, Mean pressure gradients across the aortic valve, determined by Doppler echocardiography. At 12 months there was a 49% lower mean gradient in the *Ldlr*$^{-/-}$/E06-scFv mice (2.4±1.9mmHg vs. 4.8±2.4mmHg, mean±SD, p = 0.026, *Ldlr*$^{-/-}$/E06-scFv (n=10) and *Ldlr*$^{-/-}$ (n=9). **c, d**, Calcification in aortic valve leaflets was determined by von Kossa staining of serial aortic valve sections and AUC compared. AV calcium was reduced in *Ldlr*$^{-/-}$/E06-scFv mice by 41.5% (p=0.045, one-tailed-t-test, *Ldlr*$^{-/-}$/E06-scFv (n=9) and *Ldlr*$^{-/-}$ (n=8)). **e**, Survival of mice used in AV hemodynamic study over 15 months. **f**, Hepatic cholesterol and triglyceride (TG) levels were reduced by 42% and 47% respectively in *Ldlr*$^{-/-}$*/E06-scFv* mice, *Ldlr*$^{-/-}$ (n=10) and *Ldlr*$^{-/-}$/E06-scFv (n=12) mice **g**, Livers of mice fed HCD for 16-wks were immunostained with biotinylated E06 IgM (brown) and compared to chow-fed C57BL/6 mice. Shown are representative photomicrographs, representative of 7 *Ldlr*$^{-/-}$*, 7 Ldlr*$^{-/-}$*/*

E06-scFv and 3 WT (C57BL/6) mice. **h**, Plasma serum amyloid A (SAA) was decreased 32% in HC fed *Ldlr*$^{-/-}$/E06-scFv mice (*Ldlr*$^{-/-}$ (n=10) *and Ldlr*$^{-/-}$/E06-scFv (n=12) mice).